Thesis

Fluctuations in Charge Ordering Phenomena

Kazuyoshi Yoshimi

Department of Physics
Graduate School of Science
University of Tokyo

December, 2008

Acknowledgments

I would like to express my sincerest gratitude to Professor Takeo Kato and Hideaki Maebashi for continuous encouragement and invaluable discussions during the course of the present study. I also would like to Prof. Hatsumi Mori for stimulating and helpful discussions.

I express my thanks to all the members of Kato, Mori, Takada and Ueda group for their various help.

Finally, I acknowledge my parents, brother and sisters for their continual encouragement and financial supports.

Abstract

In this thesis, we study charge-ordering phenomena by a two-dimensional extended Hubbard model with nearest-neighbor Coulomb interaction. We first formulated a non-skeleton conserving approximation and applied it to study how charge fluctuation affects charge and spin susceptibilities. We find enhancement of the spin susceptibility toward charge-ordering transition. We also calculated response functions by a self-consistent conserving approximation. The charge compressibility diverges just before the charge-ordering transition, and becomes even negative after divergence. This negative charge compressibility indicates instability of a uniform electron states, and may provide a key to understand inhomogeneous charge disproportion observed in several two-dimensional organic conductors like θ-(BEDT-TTF)$_2$RbZn(SCN)$_4$ and β-(*meso*-DMBEDT-TTF)$_2$PF$_6$.

Contents

Chapter 1

Introduction

Low-dimensional organic conductors are known to exhibit a variety of interesting electronic properties such as superconductivity, magnetism and charge-ordering etc. [1] Regardless of apparent complexity of crystal structures, many classes of organic conductors can be understood by a single-band model starting with the HOMO or LUMO molecular orbits. Unique electronic properties observed in molecular solids originate from the nature of these HOMO(LUMO) molecular orbits. Because of the large molecular orbits, organic conductors possess the following peculiar features. (1) *Softness.* The weak van der Waals bonding between molecules leads to large deformation with respect to external pressure or chemical pressure induced by substitution of cations or anions. (2) *Cleanness.* The crystal of molecular solids includes little impurity like defects due to the nature of van der Waals bonding between large molecules. (3) *Long-range Coulomb interaction.* The effective on-site interaction is relatively small compared with the inter-site Coulomb interaction because screening is weak due to the extended nature of molecular orbits.

Among a variety of phase transitions appearing in organic conductors, charge-ordering (CO) phenomena, which are a main target in this thesis, have recently attracted much attention in strongly correlated electron systems. One possible mechanism of charge-ordering is the Wigner crystallization due to long-range Coulomb repulsion. Charge disproportion in the CO phase has first been reported by NMR measurement in quasi-one dimensional

material $(\text{DI-DCNQI})_2\text{Ag}$ [2]. After this discovery, a number of experimental studies has been performed to clarify the CO in quasi-one-dimensional material such as $(\text{TMTTF})_2X$ and quasi-two-dimensional material such as α-$(\text{BEDT-TTF})_2\text{I}_3$, θ-$(\text{BEDT-TTF})_2MM'(\text{SCN})_4$ (M = Rb, Cs, M' = Zn, CO) and β-(*meso*-DMBEDT-TTF)$_2\text{PF}_6$ [3]. The experiments have shown clear evidence of long-range CO accompanied with charge disproportion in low-temperature insulator phases of these materials. These experiments, however, also have provided several unsolved questions on CO phenomena especially in quasi-two-dimensional systems.

As a typical example, we consider the quasi-two-dimensional system θ-$(\text{BEDT-TTF})_2\text{RbZn}(\text{SCN})_4$ (abbreviated as the RbZn-system in the following). This system shows a metal-insulator transition characterized by rapid exponential increase of resistance below $T_{\text{MI}} = 195\text{K}$ [4]. The spin susceptibility shows a broad peak around the metal-insulator transition with no anomaly. A paramagnetic phase is kept down to 30K where a spin-gap behavior indicating the spin-Peierls transition appears. This behavior of the uniform spin susceptibility above 30K is analyzed by the Bonner-Fisher curve of the Heisenberg model, which is an effective model of localized electrons. Although this analysis may be justified in the insulator phase, it is nontrivial to apply it to the metallic phase above T_{MI}. It is also clear that this effective spin model cannot treat the effect of charge disproportion and its fluctuation properly. In the mean-field calculation, which is a frequently used approximation for the CO phenomena, the spin susceptibility is expected to show a temperature-independent Pauli paramagnetism in the metallic phase. Therefore, one may consider the spin susceptibility from the weak-coupling perturbative approach starting with the metallic state and incorporate charge fluctuation into it. This approach has not been studied well in the previous theoretical studies of the CO phenomena.

Another question is related to the charge disproportion around T_{MI}. In the low-temperature insulator phase of the RbZn-system, stripe-type long-range CO is observed by the X-ray diffraction measurement [5, 6]. ^{13}C-NMR measurement has also shown a large charge disproportion in the CO phase [7]. However, anomalous broadening of ^{13}C-NMR spectrum observed above T_{MI} revealed a new feature of CO in this system. Such a broadening is unusual

since the metal-insulator transition is of first order. By detailed analysis of both transverse and longitudinal relaxation rates, this broadening has attributed to large fluctuation of charge disproportion in space, indicating that the fluctuation should be extremely slow ($<$ 6KHz) [8]. Similar inhomogeneous charge disproportion above $T_{\rm MI}$ have been reported by infrared and Raman spectrum [9] and dielectric measurement [10]. This strange state is often called as simply "short-range charge-ordering" without defining it exactly. By theoretical works based on the atomic limit [11], the Hartree-Fock approximation [12], the exact diagonalization [13] and the variational Monte Carlo method [14], it is suggested that several CO phases with different patterns becomes almost degenerate. This degeneracy, which indicates domain formation with different CO states, may be relevant to the so-called short-range CO. It, however, seems that essential discussion on domain formation of different CO states in a clean system is lacked.

Motivated by the above experimental results of CO in organic conductors, we investigate the effect of charge fluctuations near CO instability by the weak-coupling approach equipping a sophisticated diagrammatic expansion. Starting with an extended Hubbard model including the nearest-neighbor Coulomb interaction, we calculate the spin and charge susceptibilities by careful consideration of the vertex corrections in order to satisfy various conservation laws through the Ward identity. We show that enhancement of the spin susceptibility toward the CO transition may be understood by leading contribution of the vertex corrections. We also show that the uniform charge compressibility becomes negative just before CO transition by self-consistent treatment of large charge fluctuations. The latter result, which indicate instability of the electronic system, may give one possible explanation of inhomogeneous charge disproportion observed in organic conductors.

This thesis is organized as follows. In Chapter 2, we describe the experimental and theoretical reviews on CO in quasi-two-dimensional organic conductors. In Chapter 3, we first formulate systematic inclusion of the vertex corrections in the response functions. Then, we study the leading contribution of the vertex corrections in order to study the behavior of the spin and charge susceptibility near CO transition. In order to consider the feedback effect of critical charge fluctuation onto the Green's function, we formulate

the self-consistent treatment based on the shielded interaction approximation (SIA) in Chapter 4. We discuss the CO transition by the response function for all the wave numbers by neglecting the vertex correction. We further calculate the uniform charge compressibility including all the vertex corrections within SIA by calculating derivative of the charge number with respect to the chemical potential, and show that the charge compressibility diverges and even becomes negative just before the CO instability. The results are summarized in Chapter 5.

Chapter 2

Overview of charge-ordering in organic conductors

2.1 Electronic properties of charge-ordering phenomena

Low-dimensional organic conductors exhibit various electronic properties such as superconductivity, magnetic and charge-ordering. In particular, charge-ordering phenomena have recently attracted attention to understand effects of the long-range Coulomb interaction on strongly correlated electron systems[1, 3]. Since the molecular orbital of organic conductors is large, the wave function is extended and the on-site Coulomb repulsion U is expected to be suppressed. Therefore, the inter-site Coulomb repulsion V is expected to be comparable to U in organic conductors. It is thought that V is a key to understand the charge-ordering transition. Therefore, the extended Hubbard model (EHM) with inter-site Coulomb potential is often used to analyze charge-ordering phenomena.

In this section, we first review typical materials which exhibit charge-ordering transition in (BEDT-TTF)$_2X$ salts (abbreviated as (ET)$_2X$) where X represents different atoms or molecules. Next, we review several theoretical studies based on EHM.

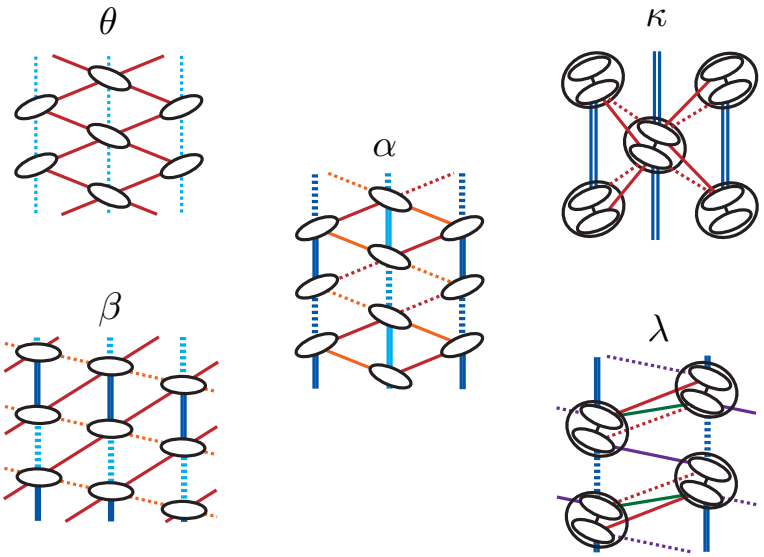

Figure 2.1: Schematic figure of five patterns of ET salts. The oval represents an ET molecule. The dotted and solid line represent the transfer integral between molecules. The circle around two molecules in κ and λ represent a dimer unit.

2.1.1 Experimental review

ET salts have the alternative layers of X^- with the closed shell and $ET^{+1/2}$ with 3/4 filled π-band. There are five patterns classified by arranging patterns of molecules labeled by the Greek characters α, β, θ ,κ and λ as shown in Fig. 2.1[15]. Among them, we focus on θ-type ET salts to review charge-ordering transition.

The electronic property of θ-$(ET)_2X$ salts is related to the dihedral angle ϕ between ET molecules[4]. Fig. 2.2 shows the schematic phase diagram experimentally obtained. The materials in the region of large ϕ such as θ-$(ET)_2$ $RbX(SCN)_4$ (X = Zn, CO) exhibit metal-insulator (MI) transition around $T_{CO} \approx 200$ K. This transition accompanies with the lattice modulation. The uniform spin susceptibility χ_s changes only slowly increases and has a broad hump at T_{CO}[16]. With decreasing the temperatures below T_{CO}, χ_s behaves like a low-dimensional localized spin system and a spin

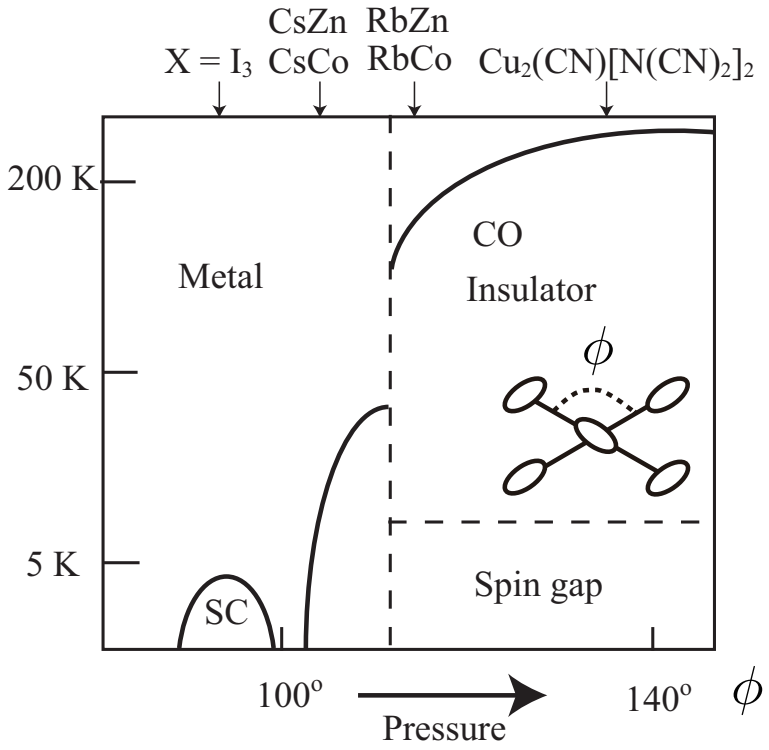

Figure 2.2: Schematic phase diagram of θ-$(ET)_2X$ salts on temperature T and dihedral angle ϕ[4]. CO and SC represent charge ordered and superconductivity state, respectively.

gapped behavior is observed below around 10 K[7]. It is notable that the existence of the short-range charge order above $T > T_{CO}$ is suggested by X-ray scattering[5]. An anomalous broadening occurs is also observed by NMR for these temperatures[8]. On the other hand, the materials in the region of smaller ϕ such as θ-$(ET)_2CsX(SCN)_4$ (X=Zn, CO), a sharp MI transition is not observed. However, with decreasing temperatures, the resistivity ρ gradually increases below around 50 K, while χ_s changes the behavior from Pauli paramagnetic to Curie-like behavior at this temperature. With the further decrease of ϕ, the charge-ordering transition does not occur and the superconducting state appears below about 5 K for θ-$(ET)_2I_3$[17].

The similar kind of ET salt β-(*meso*-DMBEDT-TTF)$_2PF_6$ also occurs the

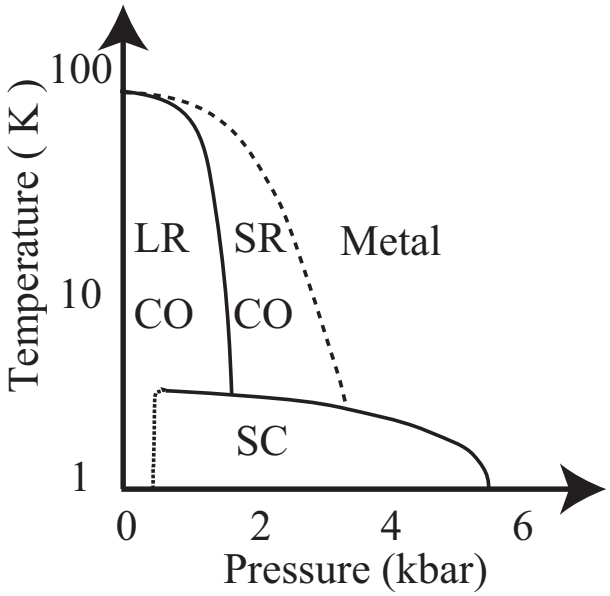

Figure 2.3: Schematic phase diagram of β-(*meso*-DMBEDT-TTF)$_2$PF$_6$ on temperature and pressure[21]. SRCO, LRCO and SC represent short-range charge ordered, long-range charge ordered and superconductivity state, respectively.

charge-ordering transition[18, 19, 20]. Fig. 2.3 shows the (P, T) phase diagram for β-(*meso*-DMBEDT-TTF)$_2$PF$_6$. At ambient pressure, the resistivity ρ shows a metallic behavior above 120 K. With decreasing temperatures, ρ gradually increases below 120 K and MI transition occurs at $T_{MI} \approx 70$ K. On the other hand, the magnetic susceptibility has a broad hump around $T_{\rm MI}$. The X-ray measurements shows that the intensity of superstructure reflections $(h, k/2, l/2)$ gradually increases below 100 K and suddenly increases at T_{MI} with decreasing temperatures. From the superstructure reflections, it is found that the insulating state exhibits the checkerboard-type charge-ordering where the charge disproportion occurs within the dimer unit. β-(*meso*-DMBEDT-TTF)$_2$PF$_6$ exhibit SC state next to the CO state with the transition temperature $T_{\rm c} \approx 4.6$ K under the pressure $P \approx 0.6$ kbar [21]. The pressure dependence of the SC state is observed below 5.2 kbar and

have found that the SC state is suppressed with increasing pressure. It is important to note that both ρ and the intensity of superstructure reflections gradually increase before the long range order transition occurs. It is proposed by Mori that this strange behavior is due to the growth of short range order and is related to the giant non-linear conductivity[22].

2.1.2 Theoretical review

To investigate the charge-ordering transition, there are several theoretical works based on the extended Hubbard model (EHM) in which the effect of the long-range Coulomb interaction is represented only by the nearest-neighbour repulsive interaction[23]

$$\mathcal{H} = \sum_{\langle ij \rangle, \sigma} t_{ij} c^{\dagger}_{i,\sigma} c_{j,\sigma} + \frac{U}{2} \sum_{i,\sigma} n_{i\sigma} n_{i\bar{\sigma}} + \sum_{\langle ij \rangle} V_{ij} n_i n_j, \tag{2.1}$$

where $\langle ij \rangle$ is the summation over neighboring pairs, t_{ij} is a transfer integral between neighboring sites. $c^{\dagger}_{i\sigma}$ ($c_{i\sigma}$) is the creation (annihilation) operator of an electron on i site with a spin σ ($= +(-)$ for $\uparrow$ ($\downarrow$)). U and V_{ij} are interaction strength for the on-site and inter-site Coulomb repulsion, respectively.

The ground state of the EHM on quarter filled square lattice was studied by a numerical Lanczos Exact Diagonalization(LED) method for cluster size up to $L = 16$ by Ohta *et al*[24]. They have shown that the checker-board type CO (CBCO) state is realized for some parameter regions. To investigate the electronic property of CBCO state, Calandra *et al* evaluated the Drude weight by a numerical LED method for cluster size up to $L = 20$ [25]. They found that the CO metallic state exists between the uniform metallic and the CO insulator state. The existence of the CO metallic state at finite temperatures has also been suggested by a dynamical mean field approximation[26] and correlator projection method[27]. However, there is a possibility that the finite size effect may be important in these calculations, since a lattice size is strongly restricted in the case of LED method. Therefore, it is expected that the charge fluctuations are not fully taken into account. Furthermore, it is difficult to investigate the various spatial patterns of CO states for LED method.

To investigate the spatial patterns of the CO states, mean-field approximation (MFA) was applied [28, 12] and succeeds to obtain various spatial patterns of the CO states. A phase diagram was also determined in the MFA to the thermodynamic potential[29, 30, 31]. In the MFA phase diagram, the static charge response function in the random-phase approximation (RPA) diverges at some ordering wave number along the second-order transition

line. An effect of fluctuations due to this divergence of the RPA charge response function for superconductivity is also investigated[29, 30, 31]. It has been shown that charge fluctuations favor to stabilize d-wave SC state. This tendency has also been found by Fluctuation Exchange (FLEX) study[32]. An effect of fluctuations due to this divergence of the RPA charge response function on the self-energy was discussed to find an anomalous T-dependence of the effective mass[33]. Effects of charge fluctuations on the uniform spin susceptibility have studied by auxiliary-field Monte Calro method for lattice sizes up to $N = 12^2$ [34]. In this method, the uniform spin susceptibility seems to follow the Curie-Weiss law and have no singularity at CO transition. However, the quantum fluctuations may be not fully treated in this method, since the low temperature region cannot be accessed due to the negative sign problem.

In the theoretical studies above mentioned, effects of charge fluctuations on the response functions have not been studied well at low temperatures. Generally, in calculating these response functions, not only the self-energy but also the vertex corrections are indispensable for satisfying some exact relations such as conservation laws. In this thesis, we investigate the vertex corrections to the charge and spin response functions in the 2D EHM at the 3/4-filling.

Chapter 3

Enhancement of spin susceptibility toward charge-ordering transition

3.1 Introduction

The vertex corrections to the charge and spin response functions were studied for the two-dimensional (2D) Hubbard model in the absence of the inter-site Coulomb interaction, corresponding to the limiting case of $V = 0$ in the extended Hubbard model (EHM). In this limiting case, there is no charge-ordering transition, but anti-ferromagnetic spin fluctuations are developed near the half-filling. It has been shown that the uniform charge susceptibility χ_c is strongly enhanced due to the nested anti-ferromagnetic spin fluctuations through the so-called Aslamazov-Larkin type vertex corrections[35, 36]. Likewise, it is expected that charge fluctuations have some contribution to the spin susceptibility near charge-ordering transition, though the spin fluctuations is weak at 3/4-filling.

In this chapter, we investigate the vertex corrections to the charge and spin response functions in the 2D EHM at the 3/4-filling in the presence of the nearest-neighbor Coulomb interaction. By calculating the static response functions at an arbitrary wave number vector, we consider effects of the vertex corrections on the charge-ordering temperature $T_{\rm CO}$ and the

uniform charge (spin) susceptibility χ_c (χ_s). Note that there exists a celebrated Baym-Kadanoff (BK) scheme for a conserving approximation, where the thermodynamic potential, the self-energy and the response functions can be constructed in a self-consistent way[38, 39]. It is, however, difficult to obtain the static response functions for all the wave numbers in the BK scheme for practical reasons. In this chapter, we introduce another scheme to formulate systematic inclusion of the vertex corrections which enables us to make actual calculations (the details are shown in Appendix). We apply this scheme to the EHM on the 2D square lattice. After determining the charge-ordering transition line in a T-V phase diagram, we obtain χ_c and χ_s in the uniform metallic phase near this transition line. Next, we explain the results of χ_c and χ_s in terms of the Landau parameters in the Fermi liquid theory. Finally, the results are summarized.

3.2 Formulation

3.2.1 Exact relations for Green's function

In this section, we consider a generic single-band Hamiltonian $\mathcal{H}$ on a lattice with band dispersion $\varepsilon_{\boldsymbol{k}}$ and electron-electron interaction $v_{\sigma\sigma'}(\boldsymbol{q})$ to formulate systematic inclusion of vertex corrections:

$$\begin{aligned}\mathcal{H} = &\sum_{\boldsymbol{k},\sigma}(\epsilon_{\boldsymbol{k}} - \mu_\sigma)c^\dagger_{\boldsymbol{k},\sigma}c_{\boldsymbol{k},\sigma} \\ &+ \frac{1}{2\Omega}\sum_{\sigma,\sigma'}\sum_{\boldsymbol{k},\boldsymbol{k}',\boldsymbol{q}} v_{\sigma\sigma'}(\boldsymbol{q})c^\dagger_{\boldsymbol{k}+\boldsymbol{q},\sigma}c^\dagger_{\boldsymbol{k}'-\boldsymbol{q},\sigma'}c_{\boldsymbol{k}',\sigma'}c_{\boldsymbol{k},\sigma}\,, \end{aligned} \tag{3.1}$$

where Ω is the volume of the lattice system, $c^\dagger_{\boldsymbol{k}\sigma}$ ($c_{\boldsymbol{k}\sigma}$) is the creation (annihilation) operator of an electron with a wave number vector $\boldsymbol{k}$ and a spin σ ($= +(-)$ for $\uparrow$ ($\downarrow$)). Because of usefulness for describing the exact relations, we have introduced $\mu_\sigma = \mu + \sigma h$ with μ and h being a chemical potential and an external magnetic field, respectively.

The charge and spin densities for the Hamiltonian $\mathcal{H}$ are given by $n = \sum_\sigma n_\sigma$ and $m = \sum_\sigma \sigma n_\sigma$, respectively. Here, n_σ is the electron number density for a spin σ; n_σ can be related to the single-particle Green's function $G_\sigma(k)$ by

$$n_\sigma = \int_k \mathrm{e}^{\mathrm{i}\epsilon_l\eta}G_\sigma(k), \tag{3.2}$$

where $\int_k$ denotes $(T/\Omega)\sum_k = (T/\Omega)\sum_{\boldsymbol{k}}\sum_l$ with k being a combined notation of a wave number vector $\boldsymbol{k}$ and a fermionic Matsubara frequency $\mathrm{i}\epsilon_l = (2l+1)\pi\mathrm{i}T$ with an integer l, and η is a positive infinitesimal. We can write $G_\sigma(k)$ as

$$G_\sigma(k) = \frac{1}{\mathrm{i}\epsilon_l + \tilde{\mu}_\sigma - \varepsilon_{\boldsymbol{k}} - \tilde{\Sigma}_\sigma(k)}\,, \tag{3.3}$$

where $\tilde{\mu}_\sigma$ absorbs the chemical potential shift due to the mean-field (Hartree) term in the self-energy $\Sigma_\sigma(k)$ as

$$\tilde{\mu}_\sigma = \mu_\sigma - \sum_{\sigma'} v_{\sigma\sigma'}(\boldsymbol{0})n_{\sigma'}, \tag{3.4}$$

and $\tilde{\Sigma}_\sigma(k)$ is the excess self-energy, which is calculated by subtracting the mean-field term from the total self-energy $\Sigma_\sigma(k)$.

The charge and spin response functions are related to the density-density response function $\chi_{\sigma\sigma'}(q)$ as

$$\chi_{NN}(q) = \frac{1}{2}\sum_{\sigma,\sigma'}\chi_{\sigma\sigma'}(q), \tag{3.5a}$$

$$\chi_{S_zS_z}(q) = \frac{1}{2}\sum_{\sigma,\sigma'}\sigma\sigma'\chi_{\sigma\sigma'}(q), \tag{3.5b}$$

where q represents a combined notation of a wave number vector $\boldsymbol{q}$ and a bosonic Matsubara frequency $\mathrm{i}\omega_l = 2l\pi\mathrm{i}T$ with an integer l; $\chi_{\sigma\sigma'}(q)$ can be written in terms of the one-interaction irreducible part $\tilde{\chi}_{\sigma\sigma'}(q)$ as

$$\chi_{\sigma\sigma'}(q) = \tilde{\chi}_{\sigma\sigma'}(q) - \sum_{\sigma_1,\sigma_2}\tilde{\chi}_{\sigma\sigma_1}(q)v_{\sigma_1\sigma_2}(\boldsymbol{q})\chi_{\sigma_2\sigma'}(q), \tag{3.6a}$$

$$\tilde{\chi}_{\sigma\sigma'}(q) = -\int_k G_\sigma(k+q)G_\sigma(k)\Lambda_{\sigma\sigma'}(k;q). \tag{3.6b}$$

Here, $\Lambda_{\sigma\sigma'}(k;q)$ is the vertex function, including the vertex corrections to the response functions.

The uniform charge and spin susceptibilities near charge-ordering are of central interest in this thesis. Here, we define these quantities (per spin) from the electron number density as $\chi_c \equiv (1/2)(\partial n/\partial\mu) = (1/2)\sum_{\sigma,\sigma'}(\partial n_\sigma/\partial\mu_{\sigma'})$ and $\chi_s \equiv (1/2)(\partial m/\partial h) = (1/2)\sum_{\sigma,\sigma'}\sigma\sigma'(\partial n_\sigma/\partial\mu_{\sigma'})$. Then, the isothermal susceptibilities χ_c and χ_s should be equal to the so-called q-limit of the charge and spin response functions, respectively:

$$\chi_c \equiv \frac{1}{2}\frac{\partial n}{\partial\mu} = \chi_{NN}(0), \tag{3.7a}$$

$$\chi_s \equiv \frac{1}{2}\frac{\partial m}{\partial h} = \chi_{S_zS_z}(0). \tag{3.7b}$$

These relations hold when both the response functions and the isothermal susceptibilities are exactly calculated. If one takes some approximation, however, these equations are not necessarily guaranteed to hold. In this chapter, we calculate the response function in an approximate form, and determine

the charge-ordering transition point by the static response functions such that

$$\chi_{NN}(\boldsymbol{q}, 0) = \infty \quad \text{at some finite } \boldsymbol{q}. \tag{3.8}$$

It is, then, desirable that the susceptibilities is calculated by the values at $\boldsymbol{q} = \boldsymbol{0}$ in the static response functions that determine the transition point in an approximation scheme, requiring that eqs. (3.7) hold. In order to construct such an approximation, it is crucial to satisfy the q-limit Ward identity

$$\Lambda_{\sigma\sigma'}(k; 0) = \delta_{\sigma\sigma'} - \frac{\partial \tilde{\Sigma}_\sigma(k)}{\partial \tilde{\mu}_{\sigma'}} \ . \tag{3.9}$$

We can show that the exact relations (3.7) hold automatically in arbitrary approximation satisfying the Ward identity (3.9) as follows. By eqs. (3.2), (3.3) and (3.4), it is not hard to see that $\partial n_\sigma / \partial \mu_{\sigma'}$ satisfies the following equation:

$$\begin{aligned}
\frac{\partial n_\sigma}{\partial \mu_{\sigma'}} &= -\int_k G_\sigma(k)^2 \sum_{\sigma_1} \left(\delta_{\sigma,\sigma_1} - \frac{\partial \tilde{\Sigma}_\sigma(k)}{\partial \tilde{\mu}_{\sigma_1}} \right) \frac{\partial \tilde{\mu}_{\sigma_1}}{\partial \mu_{\sigma'}} \\
&= -\int_k G_\sigma(k)^2 \sum_{\sigma_1} \left(\delta_{\sigma,\sigma_1} - \frac{\partial \tilde{\Sigma}_\sigma(k)}{\partial \tilde{\mu}_{\sigma_1}} \right) \\
&\quad \times \left(\delta_{\sigma_1,\sigma'} - \sum_{\sigma_2} v_{\sigma_1\sigma_2}(\boldsymbol{0}) \frac{\partial n_{\sigma_2}}{\partial \mu_{\sigma'}} \right) \ .
\end{aligned} \tag{3.10}$$

After using the Ward identity (3.9) with eqs. (3.6), we obtain the relations (3.7).

Before closing this subsection, we give some comments on a set of basic equations in the quantum many-body theory[40]. In addition to eqs. (3.6), the following equations make up this set:

$$\tilde{\Sigma}_\sigma(k) = -\sum_{\sigma'} \int_q G_\sigma(k+q) V_{\sigma\sigma'}(q) \Lambda_{\sigma\sigma'}(k; q) \, , \tag{3.11a}$$

where $V_{\sigma\sigma'}(q)$ represents the effective electron-electron interaction given by

$$V_{\sigma\sigma'}(q) = v_{\sigma\sigma'}(\boldsymbol{q}) - \sum_{\sigma_1,\sigma_2} v_{\sigma\sigma_1}(\boldsymbol{q}) \tilde{\chi}_{\sigma_1\sigma_2}(q) V_{\sigma_2\sigma'}(\boldsymbol{q}) \, . \tag{3.11b}$$

If vertex corrections are neglected, i.e. the vertex function is approximated by $\Lambda_{\sigma\sigma'}(k;q) = \delta_{\sigma,\sigma'}$ in eqs. (3.6) and (3.11), one gets renormalized RPA. It is, however, noted that neither eqs. (3.9) nor (3.7) hold in the renormalized RPA. Generic algorithm to include vertex corrections, preserving eqs. (3.9) and therefore eqs. (3.7), was proposed by Baym and Kadanoff (BK)[38, 39] on the basis of the skeleton-expansion diagrammatic analysis with respect to the dressed Green's function. In principle, the exact self-energy can be obtained from eqs. (3.6) and (3.11) combined with this BK algorithm[41].

In the following subsections, we introduce two approximations, which satisfy the Ward identity (3.9). For details of a systematic procedure for generating a series of such approximations, see Appendix A.

3.2.2 Mean-field and random-phase approximations

When the excess self-energy is neglected, the Ward identity (3.9) gives no vertex correction, i.e., $\Lambda^{(0)}_{\sigma,\sigma'}(k;q) = \delta_{\sigma\sigma'}$. This leads to MFA for the single-particle Green's function and (unrenormalized) RPA for the response functions. From eq. (3.3), the single-particle Green's function in MFA is given by

$$G^{(0)}_{\sigma}(k) = \frac{1}{\mathrm{i}\epsilon_l + \tilde{\mu}_\sigma - \varepsilon_{\boldsymbol{k}}} \,. \tag{3.12}$$

On the other hand, from eq. (3.6b), the one-interaction irreducible response function in RPA is given by

$$\tilde{\chi}^{(0)}_{\sigma\sigma'}(q) \equiv \tilde{\chi}_0(q)\delta_{\sigma,\sigma'} = -\int_k G^{(0)}_{\sigma}(k+q)G^{(0)}_{\sigma}(k)\delta_{\sigma,\sigma'} \,. \tag{3.13}$$

This approximation is, however, not suitable to the present study of the static susceptibilities; The uniform ($\boldsymbol{q} = 0$) response functions are not affected at all by charge fluctuation developed at a finite wave number $\boldsymbol{q} = \boldsymbol{Q}^*$, because the response function is calculated in a closed form for a given $\boldsymbol{q}$, and has no mode coupling.

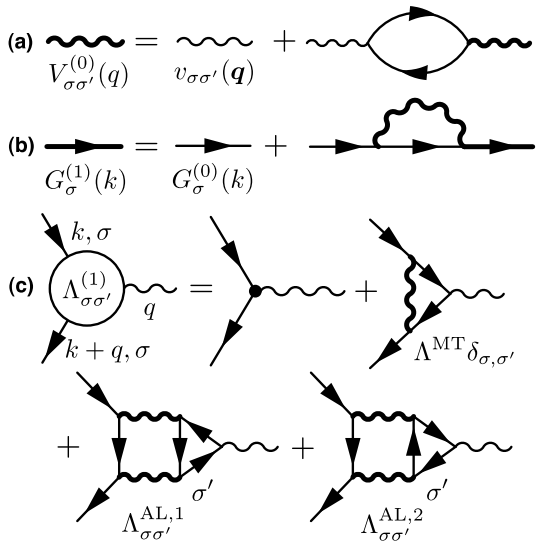

Figure 3.1: The Feynman diagram (a) for the effective electron-electron interaction $V^{(0)}_{\sigma\sigma'}(q)$, (b) for the approximate single-particle Green's function $G^{(1)}_{\sigma}(k)$, and (c) for the approximate vertex function $\Lambda^{(1)}_{\sigma\sigma'}$. The second term of r.h.s. in (c) corresponds to the Maki-Thompson-type (MT) vertex correction, while the sum of the last two terms corresponds to the Aslamazov-Larkin-type (AL) vertex correction ($\Lambda^{\rm AL}_{\sigma\sigma'} = \Lambda^{\rm AL,1}_{\sigma\sigma'} + \Lambda^{\rm AL,2}_{\sigma\sigma'}$).

3.2.3 Inclusion of vertex corrections

We start with the effective interaction of RPA as

$$V^{(0)}_{\sigma\sigma'}(q) = v_{\sigma\sigma'}(\boldsymbol{q}) - \sum_{\sigma_1,\sigma_2} v_{\sigma\sigma_1}(\boldsymbol{q})\tilde{\chi}_{\sigma_1\sigma_2}(q)V^{(0)}_{\sigma_2\sigma'}(\boldsymbol{q})\,, \tag{3.14}$$

which is expressed by the diagram in Fig. 3.1 (a). By using the effective interaction, we approximate the Green's function as

$$[G^{(1)}_{\sigma}(k)]^{-1} = [G^{(0)}_{\sigma}(k)]^{-1} - \tilde{\Sigma}^{(1)}_{\sigma}(k). \tag{3.15}$$

$$\tilde{\Sigma}^{(1)}_{\sigma}(k) = -\int_q G^{(0)}_{\sigma}(k+q)V^{(0)}_{\sigma\sigma}(q)\,, \tag{3.16}$$

where the diagram is shown in Fig. 3.1 (b).

In the present approximation, it is requested that the Ward identity (3.9) holds as discussed in § 3.2.1. For this purpose, it is essential to utilize the concept of the Hedin's formalism constructed by the skeleton diagrams, but we employ the non-skeleton diagrammatic formalism [40]. The vertex function $\Lambda^{(1)}_{\sigma\sigma'}(k;q)$ carrying a momentum q is constructed by replacing the internal $G^{(0)}_{\sigma'}(k')$ line in $\Sigma^{(1)}_{\sigma}(k)$ by $G^{(0)}_{\sigma'}(k'+q)G^{(0)}_{\sigma'}(k')$ in all the possible ways. Here, note that all the internal momenta k' are replaced so as to conserve the wave numbers and the Matsubara frequencies at all the internal and external vertices. The diagram for the vertex function thus obtained is shown in Fig. 3.1 (c). By this procedure, we can prove various types of the Ward identity, one of which is the Ward identity (3.9), i.e.,

$$\Lambda^{(1)}_{\sigma\sigma'}(k;0) = \delta_{\sigma\sigma} - \frac{\partial\tilde{\Sigma}^{(1)}_{\sigma}(k)}{\partial\tilde{\mu}_{\sigma'}}. \tag{3.17}$$

This relation is proved by seeing the fact that the differential operation in the second term on the right hand side is equivalent to an operation in which one first plucks out the internal $G^{(0)}_{\sigma'}(k')$ line in $\tilde{\Sigma}^{(1)}_{\sigma}(k)$ in all the possible ways and then replaces it with $G^{(0)}_{\sigma'}(p)^2$; this operation is nothing but the vertex insertion described above for $q = 0$.

The vertex corrections can be written as the sum of the two contributions as

$$\Lambda^{(1)}_{\sigma\sigma'}(k;q) = \delta_{\sigma,\sigma'} + \Lambda^{\mathrm{MT}}(k;q)\delta_{\sigma,\sigma'} + \Lambda^{\mathrm{AL}}_{\sigma\sigma'}(k;q)\,. \tag{3.18a}$$

The Maki-Thompson (MT) type vertex correction $\Lambda^{\mathrm{MT}}(k;q)$ is written as

$$\Lambda^{\mathrm{MT}}(k;q) = \int_{q_1} V^{(0)}_{\sigma\sigma}(q_1)G^{(0)}_{\sigma}(k+q_1+q)G^{(0)}_{\sigma}(k+q_1)\,, \tag{3.18b}$$

while the Aslamazov-Larkin (AL) type vertex correction $\Lambda^{\mathrm{AL}}_{\sigma\sigma'}(k;q)$ is written as

$$\begin{aligned}\Lambda^{\mathrm{AL}}_{\sigma\sigma'}(k;q) = \int_{q_1} & G^{(0)}_{\sigma}(k-q_1)V^{(0)}_{\sigma\sigma'}(q_1)V^{(0)}_{\sigma\sigma'}(q_1+q) \\ & \times\left[\,\gamma_{\sigma'}(q_1;q) + c.c.\,\right]\,,\end{aligned} \tag{3.18c}$$

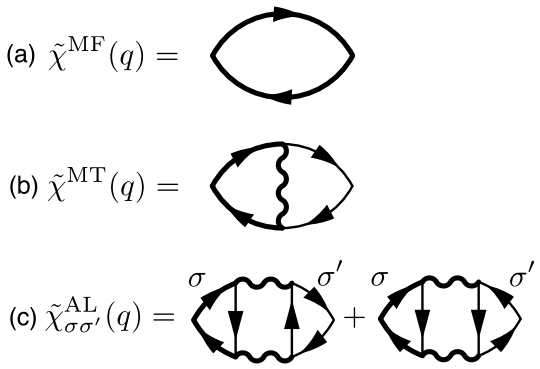

Figure 3.2: The Feynman diagrams for the one-particle irreducible response function (a) without vertex corrections, (b) with the Maki-Thompson type vertex corrections and (c) with the Aslamazov-Larkin type vertex corrections. The thin and thick solid lines with arrows represent the bare and dressed Green's functions, $G^{(0)}_\sigma(k)$ and $G^{(1)}_\sigma(k)$, respectively. The thick wavy lines represent the effective electron-electron interaction $V^{(0)}_{\sigma\sigma'}(q)$.

where $\gamma_\sigma(q_1;q)$ is the fermion loop with three vertex insertions carrying momenta q_1, q and $-q_1-q$ given by

$$\gamma_\sigma(q_1;q) = -\int_p G^{(0)}_\sigma(p)G^{(0)}_\sigma(p+q_1)G^{(0)}_\sigma(p+q_1+q)\,. \tag{3.18d}$$

The one-interaction irreducible part $\tilde{\chi}^{(1)}_{\sigma\sigma'}(q)$ in the present approximation is given as

$$\tilde{\chi}^{(1)}_{\sigma\sigma'}(q) = -\int_k G^{(1)}_\sigma(k+q)G^{(1)}_\sigma(k)\Lambda^{(1)}_{\sigma\sigma'}(k;q)\,. \tag{3.19}$$

There are three contributions in $\tilde{\chi}^{(1)}_{\sigma\sigma'}(q)$:

$$\tilde{\chi}^{(1)}_{\sigma\sigma'}(q) = \tilde{\chi}^{\rm MF}(q)\delta_{\sigma,\sigma'} + \tilde{\chi}^{\rm MT}(q)\delta_{\sigma,\sigma'} + \tilde{\chi}^{\rm AL}_{\sigma\sigma'}(q)\,. \tag{3.20}$$

The Feynman diagram for each component is shown in Fig. 3.2. Note that these diagrams are a little different from the usual ones appearing in previous literature; in both MT and AL correction, two of the Fermion lines are *dressed*

Green's functions, and the other are *bare* Green's functions. In the non-skeleton diagrammatic formalism, only this combination guarantees the exact relation (3.7) between the isothermal susceptibilities and the q-limit of the response functions through the Ward identity (3.9). The approximate spin and charge response functions are then calculated by

$$\chi_{NN}(q) = \frac{1}{2}\sum_{\sigma,\sigma'}\chi_{\sigma\sigma'}(q), \tag{3.21a}$$

$$\chi_{S_zS_z}(q) = \frac{1}{2}\sum_{\sigma,\sigma'}\sigma\sigma'\chi_{\sigma\sigma'}(q), \tag{3.21b}$$

These response functions contain a leading contribution of nontrivial vertex corrections and introduce mode coupling between charge and spin fluctuations with different wave numbers. Since the MT and AL type vertex corrections has a crucial role near a second-order transition point [35], it is expected that physically comprehensive results are obtained at this level of approximation. In the next section, we study a role of these vertex corrections near the charge-ordering transition based on this approximation.

Finally, we mention extension of the present approximation. We can construct the next level of approximation by making the next self-energy from the lastly obtained vertex function. Performing this procedure iteratively, exact series of diagrams for all the correlation functions are generated [41, 45], although it is practically difficult to sum up them. Details of this formal extension are given in Appendix.

3.3 Numerical results and discussions

3.3.1 Model

In this section, we consider a single-band EHM with the nearest-neighbor Coulomb potential for a 2D square lattice for a simple demonstration of charge fluctuation effect on the susceptibilities. The Hamiltonian is given as

$$\mathcal{H}_{\mathrm{EHM}} = \sum_{\boldsymbol{k},\sigma} (\varepsilon_{\boldsymbol{k}} - \mu) c^{\dagger}_{\boldsymbol{k}\sigma} c_{\boldsymbol{k}\sigma} + \frac{U}{2} \sum_{i,\sigma} n_{i\sigma} n_{i\bar{\sigma}} + V \sum_{\langle ij \rangle} n_i n_j. \tag{3.22}$$

The band dispersion is given as $\varepsilon_{\boldsymbol{k}} = 2t(\cos(k_x a) + \cos(k_y a))$, where t is a transfer integral between nearest-neighbor sites and a is a lattice constant. U and V are coupling constants for the on-site and nearest-neighbor repulsive Coulomb interactions, respectively. μ is determined to fix $n = \sum_\sigma n_\sigma = 3/2$ by using Eq. (3.2) and $\bar{\sigma}$ denotes the opposite spin of σ. In the following, we set $t = 1$, $a = 1$ and $k_{\mathrm{B}} = 1$.

In this model, the bare Coulomb interactions are represented as

$$v_{\sigma\sigma}(\boldsymbol{q}) = V(\boldsymbol{q}), \tag{3.23a}$$

$$v_{\sigma\bar{\sigma}}(\boldsymbol{q}) = U + V(\boldsymbol{q}), \tag{3.23b}$$

where $V(\boldsymbol{q}) = 2V(\cos q_x + \cos q_y)$. In our approximation described in 3.2.3, we obtain static charge and spin susceptibilities as

$$\chi_{NN}(\boldsymbol{q}) = \frac{\tilde{\chi}_{NN}(\boldsymbol{q})}{1 + v_c(\boldsymbol{q})\tilde{\chi}_{NN}(\boldsymbol{q})}, \tag{3.24a}$$

$$\chi_{S_z S_z}(\boldsymbol{q}) = \frac{\tilde{\chi}_{S_z S_z}(\boldsymbol{q})}{1 - U\tilde{\chi}_{S_z S_z}(\boldsymbol{q})}, \tag{3.24b}$$

where $v_c(\boldsymbol{q}) = U + 2V(\boldsymbol{q})$ has been introduced for usefulness. The one-particle irreducible response functions $\tilde{\chi}_{NN}(\boldsymbol{q})$ and $\tilde{\chi}_{S_z S_z}(\boldsymbol{q})$ are calculated from $\tilde{\chi}^{(0)}_{\sigma\sigma'}(q) = \tilde{\chi}_0(q)\delta_{\sigma,\sigma'}$ for RPA and from $\tilde{\chi}^{(1)}_{\sigma\sigma'}(q) = \tilde{\chi}^{\mathrm{SC}}(q)\delta_{\sigma,\sigma'} + \tilde{\chi}^{\mathrm{MT}}(q)\delta_{\sigma\sigma'} + \tilde{\chi}^{\mathrm{AL}}_{\sigma\sigma'}(q)$ for the approximation with the leading vertex corrections. In the rest of this thesis, the latter approximation, which is abbreviated as "the 1-st level of non-skeleton conserving approximation (1NSCA) ", is used if not specified

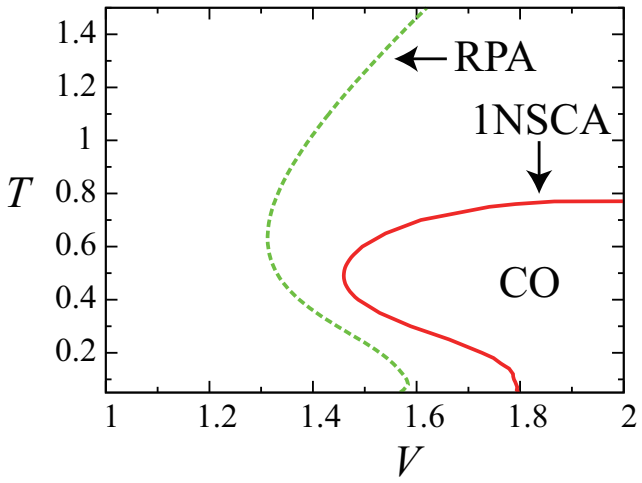

Figure 3.3: Phase diagram on the plane of T and V at $U = 3$. The dashed line and solid line represent the CO transition line determined by RPA and 1NSCA, respectively.

in the text. In order to calculate the convolution form, we use the Fast-Fourier-Transform (FFT) algorithm. The first Brillouin zone is divided into 64×64 meshes. The frequency sum is terminated at ϵ_c whose value is about 40 times as large as the band-width $W = 8t$ for $T = 0.1$. In this section, we first determine the phase diagram on the (V, T) plane. Next, we calculate the V-dependence for uniform spin and charge susceptibilities.

3.3.2 Phase diagram

In the following, we fix $U = 3$, at which a spin density wave (SDW) instability is not observed for $T \geq 0.05$. The phase diagram on the (V, T) plane at $U = 3$ is shown by a solid line in Fig. 3.4, where a charge-ordering transition is determined by the divergence of charge susceptibility, i.e., by $1 + v_c(\boldsymbol{q})\tilde{\chi}_{NN}(\boldsymbol{q}) = 0$. At high temperatures, the Fermi surface is obscure, and $\boldsymbol{q}$-dependence of $\tilde{\chi}_{NN}(\boldsymbol{q})$ is weak. As a result, checkerboard-type charge-ordering with the wave number $\boldsymbol{q} = \boldsymbol{Q}_{\rm cb} = (\pi, \pi)$ occurs mainly by $\boldsymbol{q}$-dependence of $v_c(\boldsymbol{q})$. With decreasing temperatures, the Fermi sur-

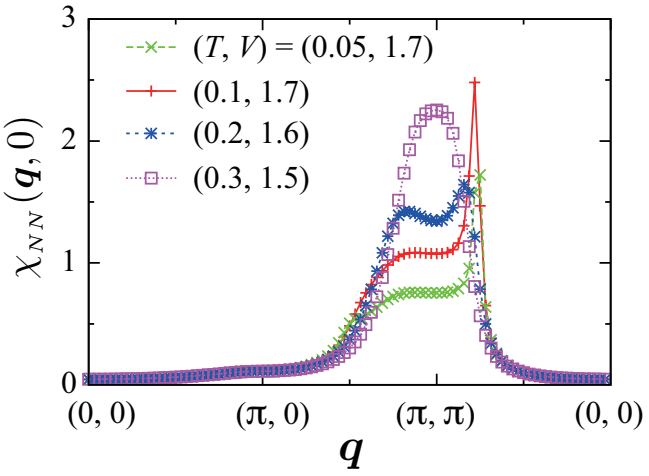

Figure 3.4: Charge susceptibilities obtained by 1NSCA for $(T, V) = (0.05, 1.7), (0.1, 1.7), (0.2, 1.6), (0.3, 1.5)$ at $U = 3$. The peak of charge susceptibility continuously shifts from $\boldsymbol{Q}_{\rm cb} = (\pi, \pi)$ to $\boldsymbol{Q}_{\rm ic} \approx (3\pi/4, 3\pi/4)$ for $T < 0.3$.

face becomes clear, and $\boldsymbol{q}$-dependence of $\tilde{\chi}_{NN}(\boldsymbol{q})$ becomes strong. Below $T \sim 0.2$, the wave number of divergence of the charge susceptibility changes from $\boldsymbol{q} = \boldsymbol{Q}_{\rm cb}$ to $\boldsymbol{q} = \boldsymbol{Q}_{\rm ic} \approx (3\pi/4, 3\pi/4)$, where the wave number $\boldsymbol{Q}_{\rm ic}$ of incommensurate charge-ordering is determined by both $v_c(\boldsymbol{q})$ and $\tilde{\chi}_{NN}(\boldsymbol{q})$. We show the charge susceptibility in the metallic phase near charge-ordering transition in Fig. 3.4. In the figure, it can be seen that the peak of the charge susceptibility shifts from $\boldsymbol{q} = \boldsymbol{Q}_{\rm cb}$ to $\boldsymbol{q} = \boldsymbol{Q}_{\rm ic} \approx (3\pi/4, 3\pi/4)$ as the temperature decreases. In the phase diagram, reentrant transition (metallic $\rightarrow$ CO $\rightarrow$ metallic with decreasing temperatures) is observed. This is due to nonmonotonic temperature-dependence of $\chi_{NN}(\boldsymbol{Q}_{\rm cb})$. Because $\boldsymbol{Q}_{\rm cb}$ is close to $\boldsymbol{Q}_{\rm ic}$, $\chi_{NN}(\boldsymbol{Q}_{\rm cb})$ first increases by broadening of the peak of $\tilde{\chi}_{NN}(\boldsymbol{q})$ at $\boldsymbol{q} = \boldsymbol{Q}_{\rm ic}$ with increasing temperatures till $T \approx 0.5$, and decreases with increasing temperatures more. As shown by the dashed line in Fig. 3.3, the overall feature of divergence of $\chi_{NN}(\boldsymbol{q})$ including reentrant behavior are also observed in RPA [29, 33]. It is noted that even considering the vertex-corrections, the reentrant charge-ordering behavior remains[46]. The vertex corrections suppress

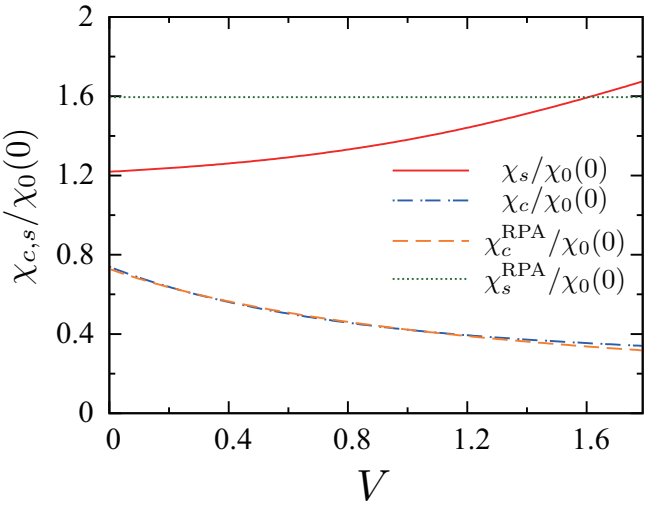

Figure 3.5: Static charge and spin susceptibility for $T = 0.1$ at $U = 3$. The dotted line and solid line represent static charge susceptibility and spin susceptibility, respectively. The incommensurate charge-ordering transition occurs at $V = 1.788$.

the CO transition especially at high temperatures because electron-electron scattering becomes strong due to obscureness of the Fermi surface. It is expected that this suppression of the CO transition may be weaken when the higher-order vertex corrections are considered. To include these terms, we have to go beyond the present approximation by, e.g., a higher level of non-skeleton conserving approximation (NSCA) discussed in Appendix A.

3.3.3 Static response functions

Let us move on the main result of this chapter. The uniform susceptibilities χ_s and χ_c calculated by RPA and the 1NSCA are shown in Fig. 3.5, where the charge-ordering transition occurs at $V = 1.788$ in the 1NSCA for $T = 0.1$ and $U = 3$. As shown in Fig. 3.5, χ_s calculated by the 1NSCA increases towards the charge-ordering transition. It is noted that χ_s is independent of V in RPA as shown in Fig. 3.5 since $\tilde{\chi}_{S_z S_z}(\boldsymbol{q}) = \chi_0(\boldsymbol{q})$ in Eq. (3.24b) does not include V. Therefore, this characteristic enhancement of χ_s is caused by

the vertex corrections. On the other hand, χ_c depends on V in both RPA and the 1NSCA as shown in Fig. 3.5, where the effect of vertex correction is small as indicated by slight change between two approximations. In the following subsections, we discuss the effect of vertex correction on χ_s and χ_c by investigating the V-dependence.

Uniform spin susceptibility

In the 1NSCA, the uniform spin susceptibility is calculated as

$$\chi_s = \frac{1}{\tilde{\chi}_{S_z S_z}(0)^{-1} - U}, \tag{3.25}$$

where $\tilde{\chi}_{S_z S_z}(0) = \tilde{\chi}_s^{\mathrm{SC}} + \tilde{\chi}_s^{\mathrm{MT}} + \tilde{\chi}_s^{\mathrm{AL}}$ is obtained as a sum of three contributions, from $\tilde{\chi}^{\mathrm{SC}}$, $\tilde{\chi}^{\mathrm{MT}}$, and $\tilde{\chi}^{\mathrm{AL}}_{\sigma\sigma'}$. From eq. (3.25), it is clear that the V-dependence of χ_s comes only from $\tilde{\chi}_{S_z S_z}(0)$ for fixed U. Therefore, χ_s is enhanced toward the charge-ordering transition by increase of $\tilde{\chi}_{S_z S_z}(0)$ for positive U. In Fig. 3.6, the V-dependence of three components, $\tilde{\chi}_s^{\mathrm{SC}}$, $\tilde{\chi}_s^{\mathrm{MT}}$, and $\tilde{\chi}_s^{\mathrm{AL}}$ are shown by subtracting their values for $V = 0$, respectively. It is found that, with increasing V, $\tilde{\chi}_s^{\mathrm{AL}}$ and $\tilde{\chi}_s^{\mathrm{MT}}$ increase, while $\tilde{\chi}_s^{\mathrm{SC}}$ decreases due to the self-energy effects.

We first discuss the behavior of $\tilde{\chi}_s^{\mathrm{MT}}$. If we consider the leading correction proportional to V and replace the dressed Green's function by the bare Green's function, $\tilde{\chi}_s^{\mathrm{MT}}$ is obtained by the integral of the interaction on the Fermi surface S_F:

$$\begin{aligned} \tilde{\chi}_s^{\mathrm{MT}} &\approx \rho^2 \int_{S_F} \mathrm{d}\boldsymbol{k}\mathrm{d}\boldsymbol{k}' V(\boldsymbol{k}-\boldsymbol{k}') \\ &= \rho^2 \langle V(\boldsymbol{q}) \rangle_{S_F}. \end{aligned} \tag{3.26a}$$

The sign of this correction depends on both $V(\boldsymbol{q})$ and the shape of the Fermi surface. In Fig. 3.7, we show the change of the Fermi surface and the corresponding averaged interaction $\langle V(\boldsymbol{q}) \rangle$ when the filling factor n is changed. In the present simple model with nearest-neighbor Coulomb interaction on a square lattice, $\langle V(\boldsymbol{q}) \rangle_{S_F}$ is positive for an arbitrary filling factor n as shown in the figure. This is because the largest contribution comes from $\boldsymbol{q} = \boldsymbol{k} - \boldsymbol{k}' \sim 0$

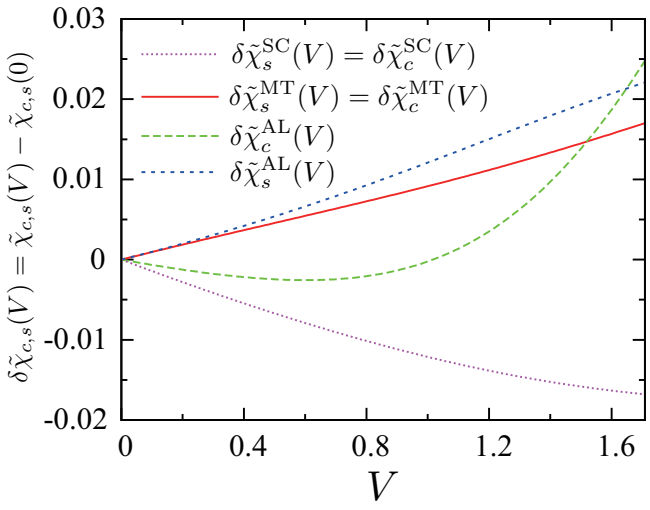

Figure 3.6: The V-dependence of irreducible static response functions is shown. for $T = 0.1$ at $U = 3$. The charge-ordering transition occurs at $V = 1.788$ in the 1NSCA.

in the integral of eq. (3.26a). Therefore, $\tilde{\chi}_s^{\rm MT}$ is expected in general to increase as V increases; this behavior is consistent with the result in Fig. 3.6.

Next, we discuss the behavior of $\tilde{\chi}_s^{\rm AL}$ in terms of the effective interaction $V_{\sigma\sigma'}^{(0)}(q) = V_{\sigma\sigma'}^{\rm RPA}(q)$. Near charge-ordering transition, the static component of the effective interaction is dominant. Therefore, $\tilde{\chi}_s^{\rm AL}$ is approximately proportional to the effective interaction,

$$\frac{1}{2}\sum_{\sigma,\sigma'}\sigma\sigma' V_{\sigma\sigma'}^{\rm RPA}(\boldsymbol{Q}^*)^2 = V_c^{\rm RPA}(\boldsymbol{Q}^*)V_s^{\rm RPA}(\boldsymbol{Q}^*). \tag{3.27}$$

Here, $V_c^{\rm RPA}(\boldsymbol{q})$ and $V_s^{\rm RPA}(\boldsymbol{q})$ are calculated as

$$V_c^{\rm RPA}(\boldsymbol{q}) = \frac{v_c(\boldsymbol{q})}{1 + v_c(\boldsymbol{q})\tilde{\chi}_0(\boldsymbol{q}, \mathrm{i}\omega_n = 0)}, \tag{3.28a}$$

$$V_s^{\rm RPA}(\boldsymbol{q}) = \frac{-U}{1 - U\tilde{\chi}_0(\boldsymbol{q}, \mathrm{i}\omega_n = 0)}, \tag{3.28b}$$

and $\boldsymbol{Q}^*$ represents the peak momentum of $V_c^{\rm RPA}(\boldsymbol{q})$. It is remarkable that $V_c^{\rm RPA}(\boldsymbol{Q}^*)$ near the CO state is negative because of $v_c(\boldsymbol{Q}^*) < 0$, while

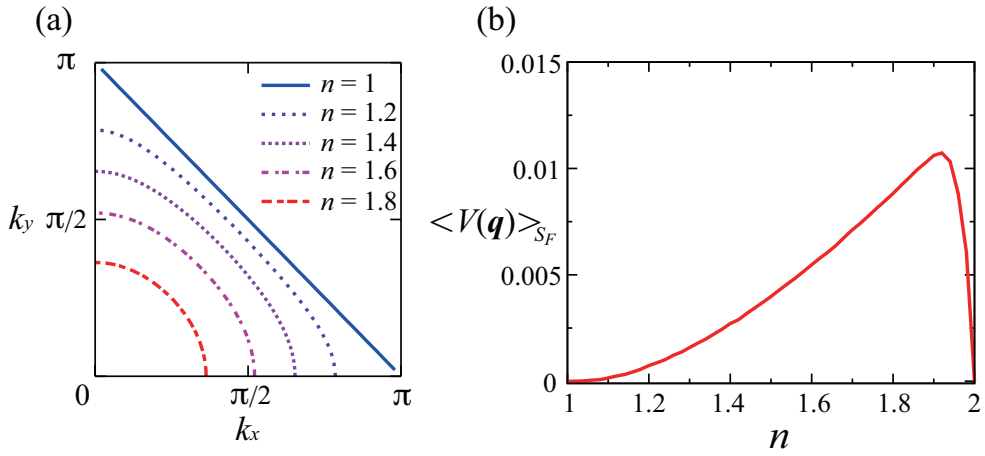

Figure 3.7: (a) The n dependence of the Fermi surface for the non-interacting system. (b) The n dependence of $\langle V(\boldsymbol{q})\rangle_{S_F}$. With increasing n, the value of $\langle V(\boldsymbol{q})\rangle_{S_F}$ increases till $n \approx 1.9$. The sharp decrease of $\langle V(\boldsymbol{q})\rangle_{S_F}$ above $n \approx 1.9$ is due to the fact that the Fermi surface becomes much small. Note that the value of $\langle V(\boldsymbol{q})\rangle$ for $0 \leq n \leq 1$ is the same as the one for $1 - n$.

$V_s^{\rm RPA}(\boldsymbol{Q}^*)$ is always negative for positive U in the absence of magnetic instability. Therefore, $\tilde{\chi}_s^{\rm AL}$ increases toward the charge-ordering transition; This behavior is consistent with the result in Fig. 3.6.

In conclusion, the charge fluctuation developed near charge-ordering transition increases the spin susceptibility through the vertex corrections; the behavior of χ_s in Fig. 3.5 can be understood qualitatively by increase of $\tilde{\chi}_s^{\rm MT}$ and $\tilde{\chi}_s^{\rm AL}$.

Uniform charge susceptibility

The uniform charge susceptibility is calculated in the 1NSCA as

$$\chi_c = \frac{1}{\tilde{\chi}_{NN}(0)^{-1} + U + 8V}, \tag{3.29}$$

where $\tilde{\chi}_{NN}(0) = \tilde{\chi}_c^{\rm SC} + \tilde{\chi}_c^{\rm MT} + \tilde{\chi}_c^{\rm AL}$ in the 1NSCA. In contrast to χ_s, the charge susceptibility is suppressed by V appearing in the denominator even in the

RPA level ($\tilde{\chi}_{NN}(0) = \tilde{\chi}_0(\mathbf{0})$). In the present calculation, V-dependence of χ_c through the vertex correction is weak as indicated from the result in Fig. 3.5. There remains, however, a possibility that the vertex correction due to the charge fluctuations affects the behavior of χ_c. Since $\tilde{\chi}_c^{\rm MT}$ is equal to $\tilde{\chi}_s^{\rm MT}$, we focus on the behavior of $\tilde{\chi}_c^{\rm AL}$. By using the same approximation as for $\tilde{\chi}_s^{\rm AL}$ in the previous subsection, $\tilde{\chi}_c^{\rm AL}$ is found to be proportional to a *square* of the effective interaction

$$\frac{1}{2}\sum_{\sigma,\sigma'} V_{\sigma\sigma'}^{\rm RPA}(\boldsymbol{Q}^*)^2 = \left[V_c^{\rm RPA}(\boldsymbol{Q}^*)\right]^2 + \left[V_s^{\rm RPA}(\boldsymbol{Q}^*)\right]^2 . \tag{3.30}$$

As a result, both $\tilde{\chi}_c^{\rm MT}$ and $\tilde{\chi}_c^{\rm AL}$ increase as V increases toward the charge-ordering transition. Therefore, χ_c is expected to increase when the vertex correction changes considerably to overwhelm the increase of $8V$ in the denominator in eq. (3.29). In order to study this possibility in details, the charge fluctuation should be fully treated beyond the present approximation. This problem will be studied in the next chapter.

3.4 Discussion

3.4.1 Relation to the Fermi liquid theory

In this subsection, the spin and charge susceptibilities are studied up to the leading-order correction derived by systematic inclusion of the vertex function. We expect that the present result gives a correct behavior of the susceptibilities toward the charge-ordering transition until the charge fluctuation is not developed so much. Just near the transition, however, the higher-order vertex correction becomes relevant due to strong charge fluctuation. Although the treatment of the higher-order correction is beyond the scope of this chapter, it is feasible to summarize its effect in terms of the Fermi liquid theory, which is a natural description of the metallic phase. By using a standard microscopic derivation of the isotropic Fermi liquid (FL), [43, 44] the irreducible part of the uniform susceptibilities is written as

$$\chi_c = \frac{\tilde{\chi}_{NN}(0)}{1 + v_c(\mathbf{0})\tilde{\chi}_{NN}(0)}, \tag{3.31a}$$

$$\chi_s = \frac{\tilde{\chi}_{S_z S_z}(0)}{1 + v_s(\mathbf{0})\tilde{\chi}_{S_z S_z}(0)}. \tag{3.31b}$$

Here, we define $v_c(0)$ and $v_s(0)$ as the spin symmetric and spin anti-symmetric parts of the bare Coulomb interaction, respectively. In FL theory, $\tilde{\chi}_c$ and $\tilde{\chi}_s$ are given as

$$\tilde{\chi}_{NN}(0) = \frac{\rho}{1 + \rho\tilde{f}_0^s}, \tag{3.32a}$$

$$\tilde{\chi}_{S_z S_z}(0) = \frac{\rho}{1 + \rho\tilde{f}_0^a}, \tag{3.32b}$$

where $\tilde{f}_0^s$ and $\tilde{f}_0^a$ are the spin symmetric and spin anti-symmetric parts of the interaction for the quasi-particle based on MF and ρ is the density for the quasi-particle on the Fermi surface. Using Eq. (3.32a) and (3.32b), Eq. (3.31a) and (3.31b) are rewritten as

$$\chi_c = \frac{\rho}{1 + \rho(v_c(\mathbf{0}) + \tilde{f}_0^s)} = \frac{\rho}{1 + \rho f_0^s}, \tag{3.33a}$$

$$\chi_s = \frac{\rho}{1 + \rho(v_s(\mathbf{0}) + \tilde{f}_0^a)} = \frac{\rho}{1 + \rho f_0^a}, \tag{3.33b}$$

where $f_0^s = v_c(\mathbf{0}) + \tilde{f}_0^s$ and $f_0^a = v_s(\mathbf{0}) + \tilde{f}_0^a$ are the spin symmetric and spin anti-symmetric parts of the quasi-particle interaction. Our formalism corresponds to approximate $|\rho\tilde{f}_0^s|, |\rho\tilde{f}_0^a| \ll 1$, where $\tilde{f}_0^s = f_0^{\mathrm{MT}} + f_0^{s,\mathrm{AL}}$ and $\tilde{f}_0^a = f_0^{\mathrm{MT}} + f_0^{a,\mathrm{AL}}$. In this limit, $\tilde{\chi}_c$ and $\tilde{\chi}_s$ are approximated as follows

$$\tilde{\chi}_c \approx \rho(1 - \rho\tilde{f}_0^s) = \rho(1 - \rho(f_0^{\mathrm{MT}} + f_0^{s,\mathrm{AL}})), \tag{3.34a}$$

$$\tilde{\chi}_s \approx \rho(1 - \rho\tilde{f}_0^a) = \rho(1 - \rho(f_0^{\mathrm{MT}} + f_0^{a,\mathrm{AL}})). \tag{3.34b}$$

From the discussion given in sec. 3.3.3, we find that all of f_0^{MT}, $f_0^{s,\mathrm{AL}}$ and $f_0^{a,\mathrm{AL}}$ decrease with the increase of charge fluctuations for a single band EHM for a square lattice model.

In the case of a single-band Hubbard model, a SDW state appears with increasing U. To consider the fact that the contribution of AL term is expected to dominate in the vicinity of a SDW state, the uniform charge susceptibility increases near a SDW state, while the spin susceptibility decreases. On the other hand, in the case of a single-band EHM with nearest-neighbor Coulomb potential, the uniform charge susceptibility decreases near a CO state, while the spin susceptibility increases as discussed in 3.3.3. However, as discussed in 3.3.3, it is noted that the charge fluctuation near a CO state is not fully taken into account and the bare Coulomb potential becomes dominant for calculating the uniform charge susceptibility in this approximation. Therefore, there is a possibility that the uniform charge susceptibility increases in the vicinity of a CO state if the charge fluctuation is fully taken into account.

3.5 Summary

In this chapter, we have developed a simple approximate method including vertex corrections which satisfy the identities between the isothermal susceptibilities and the so-called q-limit of the response functions. This method gives us a systematic phase diagram for the second-order transition and the isothermal susceptibilities by using the same response function as it should be. We showed that the reentrant charge-ordering transition, which has been observed in RPA[29], remains even though the vertex corrections are taken into account.

The notable point for including vertex corrections is that the uniform spin susceptibility increases toward the charge-ordering transition point. To interpret this tendency, we roughly evaluate the vertex-correction terms and show that this enhancement is due to decrease f_0^a from a viewpoint of Landau's Fermi Liquid theory. The experimental data such as θ-(BEDT-TTF)$_2$ $RbZn_4$[4] and β-(*meso*-DMBEDT-TTF)$_2$ PF_6[20] show that the spin susceptibility has a broad hump at the charge-ordering transition. This tendency that the spin susceptibility increases toward a CO transition point from a metallic state is consistent with our results.

On the other hand, the uniform charge susceptibility decreases toward the charge-ordering transition point. This is because that though $f_0^{\rm MT}$ and $f_0^{\rm AL}$ decrease, the bare Coulomb potential becomes dominant and f_0^s increases with increasing V. However, there is the possibility that the uniform charge susceptibility is enhanced, if the charge fluctuation is fully treated.

Chapter 4

Negative compressibility induced by large charge fluctuations

4.1 Introduction

In Chapter 3, we have constructed a new diagrammatic approach based on the non-skeleton conserving approximation including both the *bare* and *dressed* Green's function. We applied this method to the EHM to evaluate the first correction of the response function with respect to development of charge fluctuations. This correction consists of the self-energy correction and the vertex corrections of the Maki-Thompson type and the Aslamazov-Larkin type. This calculation is suitable to study of the effect of charge fluctuation on the response function toward CO transition. This approximation, however, lacks an important feedback effect of charge fluctuations onto the vertex correction of the response function.

In this chapter, we employ the Baym-Kadanoff conserving approximation (BKCA) [38, 39]. In particular, the following two aspects of the BKCA should be noted in the present context: (1) The effective interaction $V_{\rm eff}(q)$ and the self energy $\Sigma(k)$ are self-consistently determined within the skeleton diagrammatic conserving approximation. By using the Green's function thus obtained, the response function can be calculated for an arbitrary wave

number neglecting vertex corrections. This way of calculation of the response function includes Renormalized Random-Phase Approximation (RRPA) and Fluctuation Exchange (FLEX) approximation. (2) For a limited wave number $\boldsymbol{q}$, we can calculate the response function including all the vertex corrections corresponding to BKCA by derivative of the particle number with respect to the external potential[39]. Therefore, it is expected that BKCA is suitable to include the divergent increase of the effective interaction at $\boldsymbol{q} = \boldsymbol{Q}^*$ as the feedback effect onto vertex corrections near the charge-ordering critical point. For example, This aspect of the BKCA was applied to the problem of the divergent compressibility near the antiferromagnetic critical point for a 2D Hubbard model[36]. The effects of critical fluctuations on the superconductivity (SC) transition have also been well studied for a 2D extended Hubbard model by Onari *et al.* [32] in FLEX approximation. They have determined a CDW and SDW state by RRPA and discussed SC transition through charge and spin fluctuations. However, the effects of charge fluctuations on the uniform susceptibilities have not been investigated.

FLEX approximation is suitable to treat a magnetic transition, since ladder-type diagrams are included and the contribution of longitudinal spin susceptibilities is equal to that of transverse spin susceptibility. However, it is expected that the contribution of ladder-type diagrams is weak for the charge-ordering transition, since no singularity for magnetic property is expected. Actually, it is indicated that the symmetry of the SC state obtained by FLEX approximation coincides with RPA in the region where charge fluctuation is strong and spin fluctuation is weak [30]. With this observation of the validity if RPA for the CO transition, we employ RRPA [38] which subtracts ladder-type diagrams from FLEX approximation to determine the CO transition. The uniform ($\boldsymbol{q} = \boldsymbol{0}$) charge susceptibility can be calculated by $\chi_{\rm c} = {\rm d}n/{\rm d}\mu$. We call this approximation of the response function as simply the Shielded Interaction Approximation (SIA). The response function of SIA satisfies the compressibility sum rule ${\rm d}n/{\rm d}\mu = \lim_{q\to 0}\chi_{NN}(\boldsymbol{q}, 0)$. This is the crucial difference between SIA and RRPA for the calculations of the response functions. In the succeeding sections, we give the precise definition of SIA, and calculate the isothermal spin susceptibility and compressibility in SIA.

4.2 Formulation

4.2.1 Baym-Kadanoff conserving approximation

In this subsection, we briefly review BKCA. The advantage of the approximation based on Baym-Kadanoff scheme is to conserve the particle number, energy, momentum and angular momentum[38]. Baym constructed a simple formalism to procedure BKCA[39]. In this formalism, we first choose the Luttinger-Ward functional $\Phi[G]$, where $G(q)$ is the dressed Green's function given as

$$G_\sigma^{-1}(q) = \left[G_\sigma^0(q)\right]^{-1} - \Sigma_\sigma(q). \tag{4.1}$$

Here, we use the abbreviation $q \equiv (\boldsymbol{q}, i\omega_n)$, $G_\sigma^0(q)$ is the bare Green's function and the self-energy $\Sigma_\sigma(q)$ is obtained by the following relation,

$$\Sigma_\sigma(q) = \frac{\delta\Phi[G]}{\delta G_\sigma(q)}. \tag{4.2}$$

For convenience, we define $\tilde{\Sigma}_\sigma(q)$ as the self-energy subtracting the Hartree term

$$\tilde{\Sigma}_\sigma(q) = \Sigma_\sigma(q) - \Sigma_\sigma^{\mathrm{Hartree}}. \tag{4.3}$$

The vertex function $\Lambda_{\sigma_1\sigma_2}(k_1; q)$ is defined as

$$\Lambda_{\sigma_1\sigma_2}(k_1; q) = \delta_{\sigma_1\sigma_2} + \sum_{k_3,\sigma_3} \tilde{K}_{\sigma_1\sigma_3}(k_1, k_3) G_{\sigma_3}(k_3) G_{\sigma_3}(k_3 + q) \Lambda_{\sigma_3\sigma_2}(k_3; q) \tag{4.4}$$

with the irreducible kernel $\tilde{K}_{\sigma\sigma'}(q_1; q_2)$ which is given by

$$\tilde{K}_{\sigma_1\sigma_2}(q_1, q_2) = \frac{\delta\tilde{\Sigma}_{\sigma_1}(q_1)}{\delta G_{\sigma_2}(q_2)}. \tag{4.5}$$

Then, the response function is given as

$$\chi_{\sigma\sigma'}(q) = \tilde{\chi}_{\sigma\sigma'}(q) - \sum_{\sigma_1,\sigma_2} \tilde{\chi}_{\sigma\sigma_1}(\boldsymbol{q}) v_{\sigma_1\sigma_2}(\boldsymbol{q}) \chi_{\sigma_2\sigma}(q), \tag{4.6}$$

where $v_{\sigma_1\sigma_2}(\boldsymbol{q})$ represents the electron-electron interaction and $\tilde{\chi}_{\sigma\sigma'}(q)$ is defined as

$$\tilde{\chi}_{\sigma\sigma'}(q) = -\beta^{-1} \sum_k G_\sigma(k + q) G_\sigma(k) \Lambda_{\sigma\sigma'}(k; q). \tag{4.7}$$

It is noted that this formulation satisfies the Ward identity given as Eq. (3.9). For convenience, we write this relation again as follows:

$$\Lambda_{\sigma_1\sigma_2}(k_1;0) = \delta_{\sigma_1\sigma_2} - \frac{\partial\tilde{\Sigma}_{\sigma_1}(k)}{\partial\tilde{\mu}_{\sigma_2}}, \tag{4.8}$$

where $\tilde{\mu}_\sigma = \mu + h\sigma - \Sigma_\sigma^{\mathrm{Hartree}}$ is the chemical potential absorbing the Hartree term. We can see that Eq. (4.4) satisfies the Ward-identity by rewriting $\frac{\partial\tilde{\Sigma}_{\sigma_1}(k)}{\partial\tilde{\mu}_{\sigma_2}}$ in Eq. (4.8) as

$$\begin{aligned}
\frac{\partial\tilde{\Sigma}_{\sigma_1}(k)}{\partial\tilde{\mu}_{\sigma_2}} &= \sum_{k_3,\sigma_3} \frac{\partial G_{\sigma_3}(k_3)}{\partial\tilde{\mu}_{\sigma_2}} \frac{\partial\tilde{\Sigma}_{\sigma_1}(k)}{\partial G_{\sigma_3}(k_3)} \\
&= -\sum_{k_3,\sigma_3} G_{\sigma_3}(k_3)^2 \left[\delta_{\sigma_2,\sigma_3} - \frac{\partial\tilde{\Sigma}_{\sigma_3}(k_3)}{\partial\tilde{\mu}_{\sigma_2}}\right] K_{\sigma_1\sigma_3}(k,k_3) \\
&= -\sum_{k_3,\sigma_3} \tilde{K}_{\sigma_1\sigma_3}(k,k_3) G_{\sigma_3}(k_3)^2 \Lambda_{\sigma_3\sigma_2}(k_3;0).
\end{aligned} \tag{4.9}$$

Finally, we check that the the compressibility and isothermal spin susceptibility obtained from the thermodynamic potential coincides with the susceptibilities defined by Eq. (4.6)[36]. Using $\Phi[G]$, the thermodynamic potential Ω is represented as

$$\Omega = -\beta^{-1} \sum_{\boldsymbol{k},\omega_n,\sigma} \mathrm{e}^{\mathrm{i}\omega_n\eta} \left\{\ln\left[-G_\sigma^{-1}(\boldsymbol{k},\mathrm{i}\omega_n)\right] + G_\sigma(\boldsymbol{k},\mathrm{i}\omega_n)\Sigma_\sigma(\boldsymbol{k},\mathrm{i}\omega_n)\right\} + \Phi[G], \tag{4.10}$$

where η is a positive infinitesimal. The electron number n_σ is obtained by differentiating Ω with respect to the chemical potential μ_σ as

$$n_\sigma = -\frac{\partial\Omega}{\partial\mu_\sigma} = \beta^{-1} \sum_{\boldsymbol{k},\omega_n} G_\sigma(\boldsymbol{k},\mathrm{i}\omega_n)\mathrm{e}^{\mathrm{i}\omega_n\eta}. \tag{4.11}$$

Then, we can obtain the susceptibility $\chi_{\sigma\sigma'}(0)$ as

$$\chi_{\sigma\sigma'}(0) = \frac{\partial n_\sigma}{\partial\mu_{\sigma'}} = -\beta^{-1} \sum_{\boldsymbol{k},\omega_n,\sigma} \mathrm{e}^{\mathrm{i}\omega_n\eta} G_{\sigma'}^2(\boldsymbol{k},\mathrm{i}\omega_n) \left[\delta_{\sigma,\sigma'} - \frac{\partial\Sigma_\sigma(\boldsymbol{k},\mathrm{i}\omega_n)}{\partial\mu_{\sigma'}}\right]. \tag{4.12}$$

It is seen that Eq. (4.11) and (4.12) coincide with exact relations as described in sec. 3.2. The isothermal charge and spin susceptibility are defined as

$$\chi_c = \frac{1}{2}\sum_{\sigma,\sigma'}\frac{\partial n_\sigma}{\partial \mu_{\sigma'}} = \frac{1}{2}\sum_{\sigma,\sigma'}\chi_{\sigma\sigma'}(0), \tag{4.13}$$

$$\chi_s = \frac{1}{2}\sum_{\sigma,\sigma'}\sigma\sigma'\frac{\partial n_\sigma}{\partial \mu_{\sigma'}} = \frac{1}{2}\sum_{\sigma,\sigma'}\sigma\sigma'\chi_{\sigma\sigma'}(0), \tag{4.14}$$

respectively. In this way, we can obtain the compressibility and isothermal spin susceptibility which satisfy exact relations. It is noted that the vertex corrections are included through the differentiating Σ with respect to μ or δh.

4.2.2 Shielded interaction approximation

In the vicinity of charge-ordering transition, charge density fluctuations become important. To consider this effect, we choose the Luttinger-Ward functional $\Phi[G]$ as the sum of all bubble ring-diagrams as shown in Fig. 4.1 (a). Then, the self-energy $\Sigma(q)$ in Fig. 4.1 (b) is given by Eq. (4.2) as

$$\Sigma_\sigma(q) = \sum_{\sigma'} v_{\sigma\sigma'}(\boldsymbol{0})n_{\sigma'} + \beta^{-1}\sum_k V^{\mathrm{SIA}}_{\sigma\sigma}(k)G_\sigma(k+q), \tag{4.15}$$

where the shielded interaction $V^{\mathrm{SIA}}_{\sigma\sigma}(k)$ shown in Fig. 4.1 (c) is defined as

$$V^{\mathrm{SIA}}_{\sigma\sigma}(q) = -v_{\sigma\sigma}(\boldsymbol{q}) + \sum_{\sigma_1\sigma_2} v_{\sigma\sigma_1}(\boldsymbol{q})\chi^{\mathrm{RRPA}}_{\sigma_1\sigma_2}(q)v_{\sigma_2\sigma}(\boldsymbol{q}). \tag{4.16}$$

Here, $v_{\sigma\sigma}(\boldsymbol{q}) = V(\boldsymbol{q})$ and $v_{\sigma\bar{\sigma}}(\boldsymbol{q}) = U + V(\boldsymbol{q})$ are the wave representation of the Coulomb potential between the same and different spins for EHM, respectively. The susceptibility $\chi^{\mathrm{RRPA}}_{\sigma\sigma'}(q)$ is given as

$$\chi^{\mathrm{RRPA}}_{\sigma\sigma'}(q) \;=\; \tilde{\chi}^{\mathrm{SC}}_{\sigma\sigma}(q) - \sum_{\sigma_1,\sigma_2}\tilde{\chi}^{\mathrm{SC}}_{\sigma\sigma_1}(q)v_{\sigma_1\sigma_2}(\boldsymbol{q})\chi^{\mathrm{RRPA}}_{\sigma_2\sigma'}(q), \tag{4.17}$$

where $\tilde{\chi}^{\mathrm{SC}}_{\sigma\sigma'}(q)$ (SC means the Self-energy Correction) is the irreducible susceptibility for the dressed Green's function,

$$\tilde{\chi}^{\mathrm{SC}}_{\sigma\sigma'}(q) = -\beta^{-1}\sum_k G_\sigma(k)G_\sigma(k+q)\delta_{\sigma,\sigma'}. \tag{4.18}$$

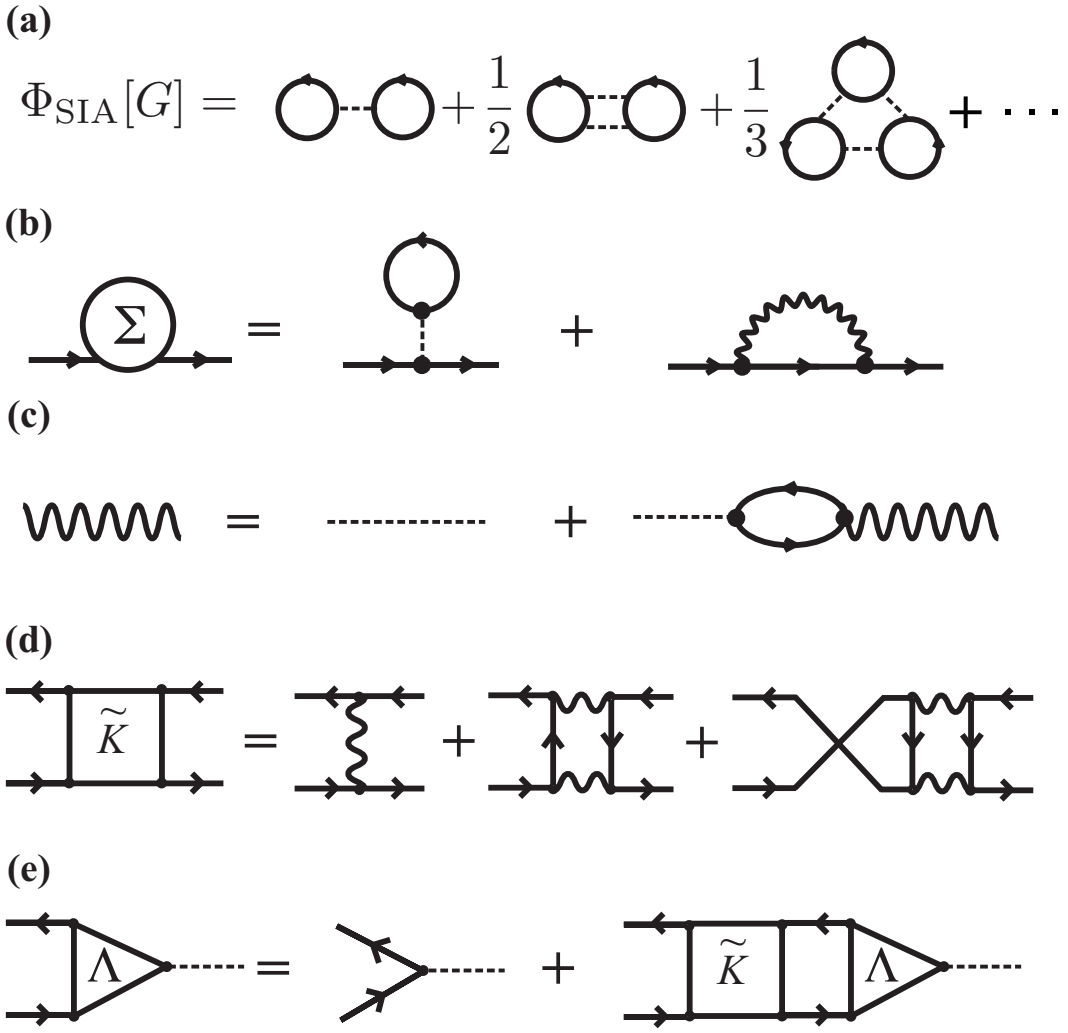

Figure 4.1: The Feynman diagrams of the SIA: (a) the Luttinger-Ward functional Φ_{SIA}, (b) the self-energy Σ, (c) the shielded interaction $V^{\mathrm{SIA}}_{\sigma\sigma}$, (c) the irreducible Kernel $\tilde{K}$ and (d) the vertex functions Λ.

In this thesis, the chemical potential μ is determined to fix the electron number $n = \sum_\sigma n_\sigma$ as $3/2$ by using Eq. (4.11) within the accuracy $|n - n_{\rm fix}| \leq 10^{-8}$. We solved coupled equations Eq. (4.1) and (4.15) iteratively until satisfying the convergence condition for each k and σ within the accuracy

$$\frac{|\Sigma_\sigma^{(i+1)}(k) - \Sigma_\sigma^{(i)}(k)|}{|\Sigma_\sigma^{(i+1)}(k)|} \leq 10^{-6}, \tag{4.19}$$

where i denotes the i-th iteration.

In SIA, the divergence of effective interaction $V_{\sigma\sigma}^{\rm SIA}(q)$ reflects on the self-energy $\Sigma(q)$. We investigate the influence of the charge fluctuations through this feedback effect. The divergence point of $V_{\sigma\sigma}^{\rm SIA}(q)$ is equivalent to that of $\chi_{NN}^{\rm RRPA}(q)$ defined as

$$\chi_{NN}^{\rm RRPA}(q) = \frac{1}{2}\sum_{\sigma\sigma'} \chi_{\sigma\sigma'}^{\rm RRPA}(q). \tag{4.20}$$

Hereafter, we define the charge-ordering transition point as the divergence point of $\chi_{NN}^{\rm RRPA}(q)$ at some finite q. It is noted that the sum rule

$$\chi_c \equiv \frac{\partial n}{\partial \mu} = \lim_{q\to 0} \chi_{NN}^{\rm RRPA}(q) \tag{4.21}$$

does not hold in RRPA, since the vertex corrections required in BKCA are not taken into account. Uniform charge susceptibility, however, can be calculated by direct derivative of the particle number with respect to the chemical potential (see l.h.s in Eq. (4.21)). Charge compressibility χ_c thus obtained should include not only Maki-Thompson (MT) and Aslamazov-Larkin (AL) type vertex corrections but also higher-order ones. Likewise, χ_s obtained by differentiating m with respect to δh also includes appropriate vertex corrections. In the next section, we investigate the effect of charge fluctuations on χ_c and χ_s in this way.

4.3 Numerical results

In this section, we take a lattice size $N = 64^2$ and the Matsubara frequency for fermions $-(2N_c-1)\pi T \leq \omega_n \leq (2N_c-1)\pi T$ with $N_c = 2^{11}$ above $T = 0.1$. While, we take $N = 128^2$ and $N_c = 2^{11}$ below $T = 0.1$.

4.3.1 Transition point determined by RRPA

In the case of $h = 0$, $\tilde{\chi}^{\rm SC}_{\sigma\sigma'}$ does not depend on the spin indices and we can define $\tilde{\chi}^{\rm SC}(q) \equiv \tilde{\chi}^{\rm SC}_{\sigma\sigma'}(q)$. Then, the charge and spin susceptibility obtained by RRPA at SIA level is rewritten as

$$\chi^{\rm RRPA}_{NN}(q) = \sum_{\sigma\sigma'} \chi^{\rm RRPA}_{\sigma\sigma'}(q) = \frac{\tilde{\chi}^{\rm SC}(q)}{1 + [U + 2V(\boldsymbol{q})]\,\tilde{\chi}^{\rm SC}(q)}, \tag{4.22}$$

$$\chi^{\rm RRPA}_{S_zS_z}(q) = \sum_{\sigma\sigma'} \sigma\sigma' \chi^{\rm RRPA}_{\sigma\sigma'}(q) = \frac{\tilde{\chi}^{\rm SC}(q)}{1 - U\tilde{\chi}^{\rm SC}(q)}. \tag{4.23}$$

We determine the charge-ordering transition by the divergence of $\chi^{\rm RRPA}_{NN}(\boldsymbol{q}, 0)$ at some finite $\boldsymbol{q}$.

First, we see the momentum dependence of $\chi^{\rm RRPA}_{NN}(\boldsymbol{q}, 0)$ and specify the wave vector $\boldsymbol{Q}^*$, where $\chi^{\rm RRPA}_{NN}(\boldsymbol{q}, 0)$ has maximum value. Fig. 4.2 (a) shows the momentum dependence of $\chi^{\rm RRPA}_{NN}(\boldsymbol{q}, 0)$ and $\chi^{\rm RRPA}_{S_zS_z}(\boldsymbol{q}, 0)$ at $U = 4$ and $T = 0.1$. Two peaks of $\chi^{\rm RRPA}_{NN}(\boldsymbol{q}, 0)$ are due to the anisotropic wave dependence of $V(\boldsymbol{q})$ and that of the Fermi surface. The former gives a peak at $\boldsymbol{q} = \boldsymbol{Q}_{cb} = (\pi, \pi)$ and the latter at $\boldsymbol{q} = \boldsymbol{Q}_{inc} = (\frac{3}{4}\pi, \frac{3}{4}\pi)$. It is seen that $\chi^{\rm RRPA}_{NN}(\boldsymbol{Q}_{cb}, 0)$ is enhanced with increasing V in this case. To determine the divergent point of $\chi^{\rm RRPA}_{NN}(\boldsymbol{Q}_{cb}, 0)$, we calculate V-dependence of $\chi^{\rm RRPA}_{NN}(\boldsymbol{Q}_{cb}, 0)$ as shown in Fig. 4.2 (b) and find that charge-ordering transition occurs at $V \approx 2.066$. We also check the V-dependence of the maximum value of $\chi^{\rm RRPA}_{S_zS_z}(\boldsymbol{q}, 0)$. With increasing V, $\chi^{\rm RRPA}_{S_zS_z}(\boldsymbol{q}, 0)$ decreases. Therefore, it is seen that the spin fluctuations are suppressed by the charge fluctuations.

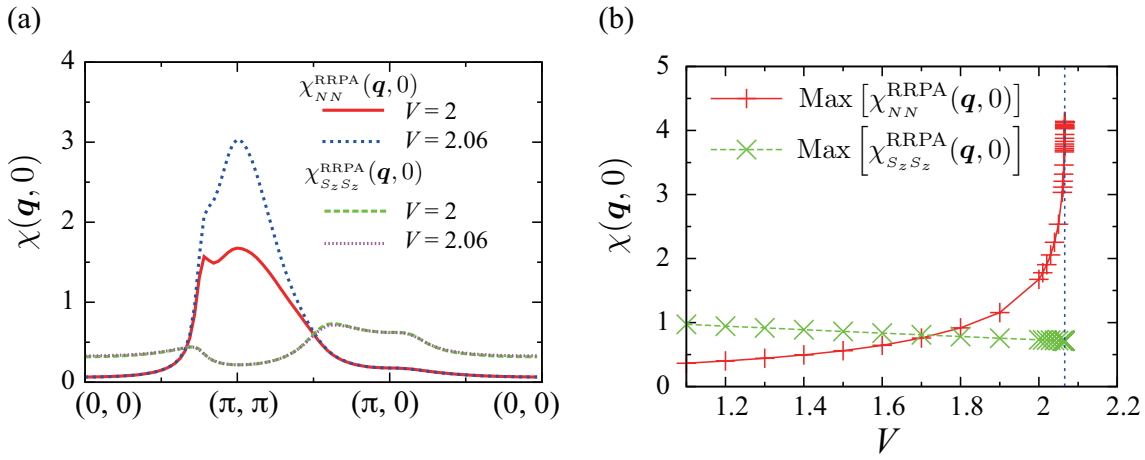

Figure 4.2: (a) The wave dependence of $\chi^{\mathrm{RRPA}}_{NN}(\boldsymbol{q},0)$ and $\chi^{\mathrm{RRPA}}_{s}(\boldsymbol{q},0)$ at $U=4$ and $T=0.1$. (b) The V dependence of Max $\left[\chi^{\mathrm{RRPA}}_{NN}(\boldsymbol{q},0)\right]$ and Max $\left[\chi^{\mathrm{RRPA}}_{s}(\boldsymbol{q},0)\right]$ at $U=4$ and $T=0.1$. The charge-ordering transition occurs about $V\approx 2.066$.

4.3.2 Response functions

In the previous subsection, we determine the charge-ordering transition point by RRPA. In this subsection, we investigate the effect of the charge fluctuations on the isothermal spin susceptibility χ_s and compressibility χ_c. To obtain χ_c, we utilize the relation Eq. (4.12). In this method, χ_c includes vertex corrections through $\frac{\partial\Sigma}{\partial\mu}$ as explained §4.2.2. Likewise, we calculate χ_s by differentiating m with respect to δh to include the vertex corrections.

Isothermal spin susceptibility

To obtain χ_s, we numerically apply a small magnetic field δh and calculate magnetization $m=\sum_\sigma \sigma n_\sigma$ by the following relation,

$$n_\sigma = \beta^{-1}\sum_{\boldsymbol{k},\omega_n} G_\sigma(\boldsymbol{k},\mathrm{i}\omega_n)\mathrm{e}^{\mathrm{i}\omega_n\eta}. \tag{4.24}$$

Fig. 4.3 (a) shows h-dependence of m at $V=1$ (red line), 2 (green line) and 2.05 (blue line). It is seen that m varies linearly near $\delta h\approx 0$ for each V.

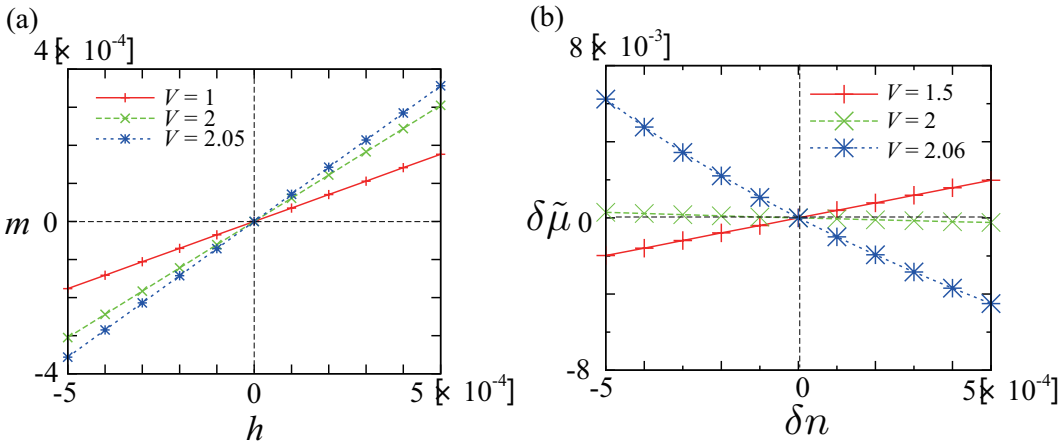

Figure 4.3: (a) Magnetic field h dependence of the magnetization m at $U = 4$ for $T = 0.1$. (b) δn dependence of $\delta\tilde{\mu} = \delta\mu - \Sigma_{\rm Hartree}$ at $U = 4$ for $T = 0.1$, where we define $\delta n = n - 1.5$ and $\delta\mu = \mu - \mu_{\rm fix}$. $\mu_{\rm fix}$ is the chemical potential determined to fix $n = 1.5$. The divergence of χ_c occurs at $V \approx 2.064$.

Therefore, we calculate χ_s by $\delta m/\delta h$, where $\delta h = 10^{-4}$.

The blue line in Fig. 4.4 (a) represents χ_0/χ_s at $U = 4$ for $T = 0.1$, where χ_0 is the compressibility for non-interaction system. With decreasing $\delta V \equiv V_{\rm CO} - V$, the charge fluctuations become large, where $V_{\rm CO}$ represents the charge-ordering transition point. Though the enhancement of charge fluctuations near $V_{\rm CO}$ is reflected on χ_s through vertex corrections, anomalous behavior is not observed and χ_s^{-1} monotonically decreases with increasing V. This tendency qualitatively coincides with the 1NSCA as discussed in Chapter 3.

Isothermal charge susceptibility

To obtain χ_c, we numerically increase the electron number density $n = 3/2$ by a small amount δn. Then, the chemical potential μ slightly changes from μ to $\mu + \delta\mu$. Fig. 4.3 (b) shows δn dependence of the chemical potential absorbing Hartree term $\delta\tilde{\mu} = \delta\mu - \delta\Sigma_{\rm Hartree}$ for $V = 1.5$ (red line), 2 (green line) and 2.06 (blue line). It is seen that δn is proportional to $\delta\tilde{\mu}$ near $\delta\tilde{\mu} \approx 0$

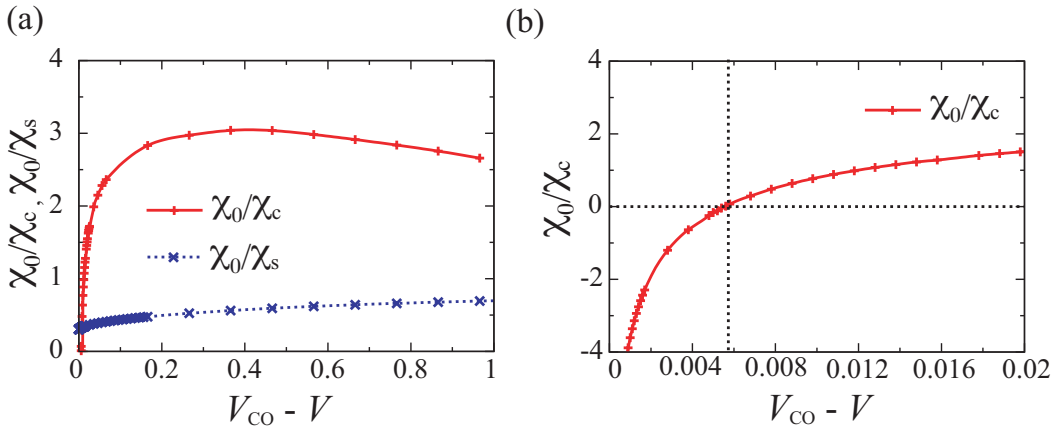

Figure 4.4: V-dependence of χ_0/χ_c and χ_0/χ_s at $U = 4$ for $T = 0.1$ in the range (a) $0 \leq V_{\rm CO} - V \leq 1$ and (b) $0 \leq V_{\rm CO} - V \leq 0.1$. Here, $V_{CO} \approx 2.066$ is defined as the charge-ordering transition point determined by RRPA. The red and green line represent χ_0/χ_c and χ_0/χ_s, respectively. The divergence of χ_c occurs at $V \approx 2.060$.

for each V. Therefore, we calculate $\tilde{\chi}_c = \delta n/\delta\tilde{\mu}$ for $\delta n = 10^{-4}$ and obtain χ_c by $\chi_c^{-1} = \tilde{\chi}_c^{-1} + U + 2V(\mathbf{0})$.

The red line in Fig. 4.4 (a) and (b) represents χ_0/χ_c at $U = 4$ for $T = 0.1$. With decreasing δV from $\delta V = 1$, χ_c^{-1} first increases till $\delta V \approx 0.3$. This result coincides with the result of 1NSCA as discussed in Chapter 3. In this region, the contribution of the bare Coulomb potential V to the compressibility is dominant and the compressibility decreases. Since the enhancement of $V_{\sigma\sigma}^{\rm SIA}(\boldsymbol{Q}_{cb}, 0)$ near V_{CO} is taken into account in SIA, it is expected that the contribution of the vertex corrections to the compressibility is dominant in the vicinity of charge-ordering transition. This tendency is appeared below $\delta V \approx 0.3$ and χ_c^{-1} becomes 0 before charge-ordering transition. This indicates that the electronic system becomes unstable due to charge fluctuations.

Next, we determine the phase diagram on the V-T plane obtained from divergence of the response function $\chi_{NN}^{\rm RRPA}(\boldsymbol{Q}^*, 0)$ responsible for a charge-ordering transition and the uniform charge compressibility χ_c. The phase diagram on the V-T plane for $U = 4$ is shown in Fig. 4.5. The blue points

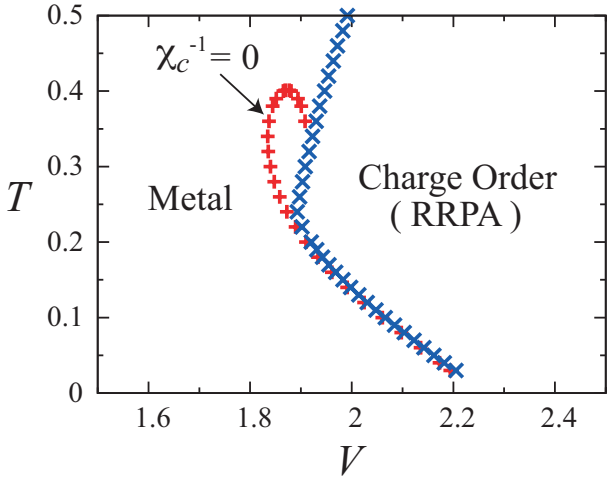

Figure 4.5: The phase diagram in the $V - T$ plane for $U = 4$ with a uniform metallic and a charge ordered state determined by RRPA. The blue points represent the charge-ordering transitions. The red points represent the divergence points of static charge susceptibility. An end point appears at $T \approx 0.401$.

represent the charge-ordering transition points on which $\chi^{\rm RRPA}_{NN}(\boldsymbol{Q}^*, 0)$ diverges. This result shows reentrant transition (metallic $\rightarrow$ CO $\rightarrow$ metallic with decreasing the temperature) in a finite region of V at RRPA level. This reentrant transition is also observed in both 1NSCA and RPA as shown in the previous chapter. The characteristic transition temperature obtained here is, however, lowered from RPA (or 1NSCA). From viewpoint of Fermi liquid, the self-energy correction included in RRPA is expected to lower the transition temperature by suppression of the response function at finite temperatures through both strong electron scattering (the imaginary part of the self-energy) and mass renormalization (the real part of the self-energy). In order to study this effect more quantitatively, careful analysis of the self-energy is needed since the response function at $\boldsymbol{q} = \boldsymbol{Q}^* = \boldsymbol{Q}_{\rm cb}$ should involve quasi-particle excitation far from the Fermi surface.

The red points in Fig. 4.5 represent $V_{ins}(T)$ where χ_c diverges for fixed T. It is seen that an end point of V_{ins} appears at $T \approx 0.401$. Fig. 4.6 shows

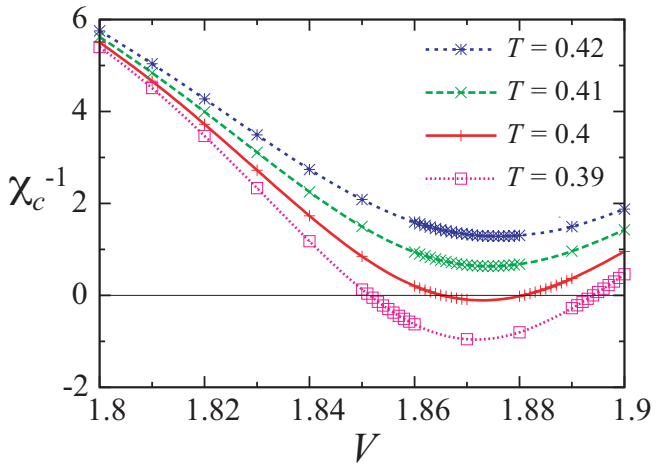

Figure 4.6: V-dependence of χ_c^{-1} at $U = 4$. The pink, red, blue and green line represent the results for $T = 0.39,\ 0.4,\ 0.41$ and 0.42, respectively. Above $T = 0.41$, the divergence of χ_c does not appear.

V-dependence of χ_c^{-1} at $U = 4$ for $T = 0.39$, 0.4, 0.41 and 0.42. It is seen that χ_c has a local minimum point at $V = V_{min}$ at fixed T. With increasing V, the effective interaction $V_{\sigma\sigma}^{\rm SIA}(\boldsymbol{Q}^*, 0)$ becomes large, while $G(q)$ decreases since the electron scattering (the self-energy correction) is enhanced. Therefore, it is expected that the decrease of the compressibility for $V > V_{min}$ is due to the effect of $G(q)$. In SIA, χ_c has higher-order terms of Aslamazov-Larkin (AL) type vertex corrections which are expected to be important for the compressibility with increasing charge fluctuations as discussed in the previous chapter. These terms have $\lambda(Q_{CB} = (\boldsymbol{Q}_{CB}, 0))$ which is defined as

$$\lambda(Q_{CB}) = -\sum_k G^2(k)G^2(k + Q_{CB}). \tag{4.25}$$

Fig. 4.7 (a) and (b) show V-dependence of $\lambda(Q_{CB})$ at $T = 0.2$ and 0.42. It is seen that $\lambda(Q_{CB})$ decreases with increasing V for both temperatures. However, the ratio of decrease of $\lambda(Q_{CB})$ is large and the value of $\lambda(Q_{CB})$ is small for high temperatures. This tendency coincides with the behavior of V_{ins} at high temperatures and it is expected that the suppression of $G(q)$ has the key to form the end point.

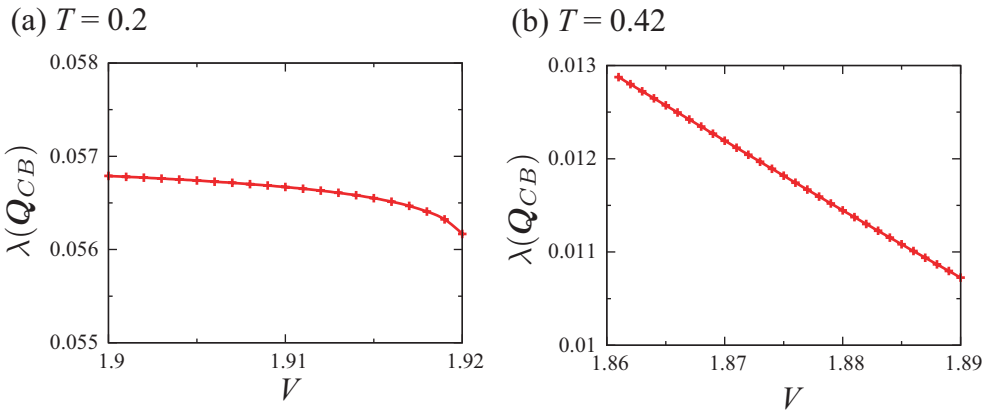

Figure 4.7: V-dependence of $\lambda(Q_{CB})$at $U = 4$ for (a) $T = 0.2$ and (b) $T = 0.42$. The charge-ordering transition point determined by RRPA is at $V_{CO} = 1.92$ for $T = 0.2$ and $V_{CO} = 1.954$ for $T = 0.42$, respectively.

4.4 Summary and discussions

In this chapter, we have shown divergence of the uniform charge susceptibility χ_c before the charge-ordering transition in the present model, i.e., 2D EHM with nearest-neighbour Coulomb interaction. The negative charge susceptibility means instability of electrons with respect to the uniform change of the electron density. One possible state is a spatially inhomogeneous state of a uniform metallic state and a charge-ordered state with different electron densities. We call this mixed state as a "phase separation". We show a schematic figure of the phase separation in Fig. 4.8. It is noted that the system is already in the phase separation before divergence of χ_c. The transition point into the phase separation should be determined by reconstruction of the nonconvex free energy by the Maxwell construction law. In the present calculation, we cannot perform this procedure because of the lack of the free energy in the charge ordered phase. The negative compressibility, however, guarantees at least the existence of the phase separation in the present model.

In order to relate this electronic instability to the experimental observation of inhomogeneous charge disproportion in organic conductors, we need careful consideration of approximation adopted in the model. Especially, the

long-range Coulomb interaction neglected in the EHM is important since the charge-rich(poor) phase with imbalance between the electron charge and the background positive charge of ions has a macroscopic charge, and therefore has a large charging energy due to long-range Coulomb interaction. We expect that in the presence of the long-range Coulomb interaction this negative compressibility drives the system into a "microscopic" inhomogeneous state rather than the macroscopic phase separation[47]. It is an important question left for a future problem to clarify the final inhomogeneous electronic state realized after electronic instability of uniform metallic state. We conjecture that strong electron-phonon coupling may play an important role to relax a kind of charge frustration induced by long-range interaction.

In this chapter, we clarified one possible realization of electronic instability starting with a metallic state by perturbative approach using diagrammatic expansion. We emphasize that the existence of the Fermi surface is essential for the instability in the present calculation. We speculate that the negative compressibility may be understood by the Pomeranchuk instability with respect to uniform change of electron density in terms of the Fermi liquid theory. Then, it is critical to ask whether the negative compressibility survives even in the presence of strong electron correlation. This is a difficult question to be answered, and have to be left for a future problem. We only note that the phase separation is obtained in the one-dimensional EHM for large positive V by exact diagonalization method [48]. Finally, we provide a complementary result for a hint of consideration of phase separation in the strongly correlated regime. In Fig. 4.9, we show the distance between two instabilities of phase separation and CO indicating the size of the phase separation region in the phase diagram for $T = 0.1$. We find that the phase separation region is suppressed when the on-site interaction U increases. This result strongly indicates that the phase separation seen in the present calculation disappears in the limit of $U \to \infty$ while fixing V. This suggests that the correct strong-coupling limit should be taken to keep a finite portion of doublon excitation if one considers phase separation in the strong coupling region.

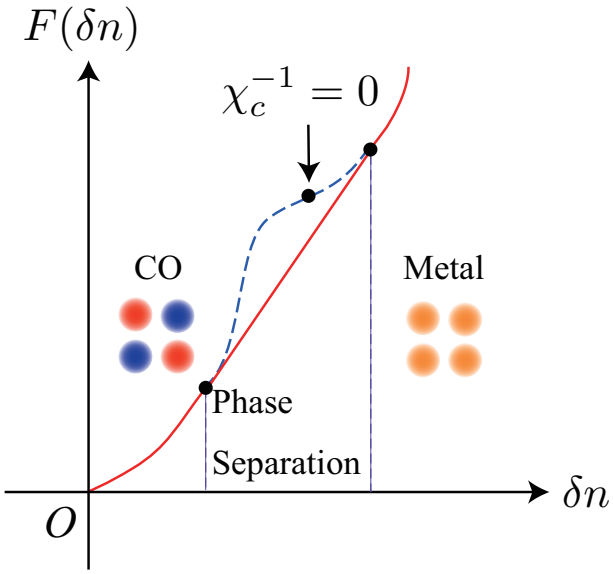

Figure 4.8: Schematic particle density ($\delta n = n - 1$) dependence of the free energy for the phase separation with uniform metal and a CO states. The concave region appears in the dashed line. This thermodynamically unstable region is replaced with the phase separated state by Maxwell construction.

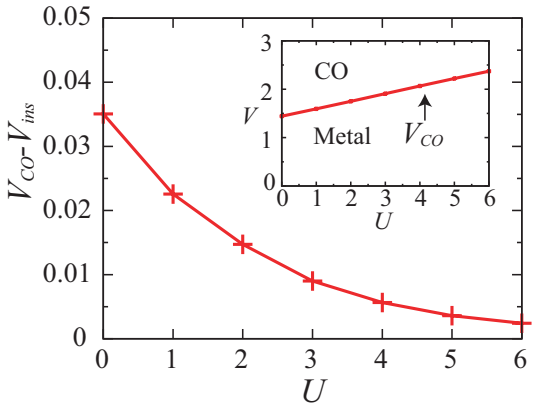

Figure 4.9: The U dependence of $V_{\mathrm{CO}} - V_{ins}$ at $T = 0.1$. The inset shows the phase diagram on (U, V) plane at $T = 0.1$. The charge-ordering transition line is determined by RRPA.

Chapter 5

Summary

In this thesis, electronic properties of organic conductors in the presence of the inter-site Coulomb interaction are investigated in the viewpoint of diagrammatic expansion starting from the metallic state.

We first studied the spin and charge response functions by using a new scheme of generating a series of non-skeleton conserving approximation(NSCA). We showed that the reentrant transition observed in RPA remains even in the first-order NSCA. We also showed that the spin susceptibility is enhanced toward the CO transition. This result is consistent with the measurement of the spin susceptibility of θ-(BEDT-TTF)$_2$RbZn(SCN)$_4$ and β-(*meso*-DMBEDT-TTF)$_2$PF$_6$.

Next, we studied the uniform charge susceptibility by using the shielded-interaction approximation within the Baym-Kadanoff conserving approximation. The merit of this approximation is that all the vertex corrections can be fully treated by direct differential calculation of the response of the system with respect to the external potential. This calculation allows us to study the feedback effect of strong charge fluctuations onto the response function through the vertex corrections. We find that the strong charge fluctuations lead to a remarkable enhancement of the charge compressibility and even make it negative indicating the instability of uniform metallic state near the CO transition. This may provide a trigger of the inhomogeneous charge disproportion called as "short-range charge-ordering" observed in the exper-

iments of θ-(BEDT-TTF)$_2$RbZn(SCN)$_4$ etc.

The present calculation has been done for a simple square-lattice EHM with nearest-neighbor Coulomb interaction. In order to compare the present theory with experiments, it is needed to consider several important effects. In particular, the long-range Coulomb interaction beyond the nearest-neighbor site and electron-phonon interaction will be important to analyze the experiments. More realistic calculation including these effects will be a future problem.

Appendix A

Non-skeleton conserving approximation

In this Appendix, we present an iterative approximation scheme for systematic inclusion of vertex corrections to the charge and spin response functions. We construct (A) the single-particle Green's function $G_\sigma^{(i)}(k)$, (B) the vertex function $\Lambda_{\sigma\sigma'}^{(i)}(k;q)$, and (C) the response functions $\chi_{NN}^{(i)}(q)$ and $\chi_{S_zS_z}^{(i)}(q)$. These functions are constructed so that Ward identity holds at each level of approximation assigned by an integer i based on the Kadanoff-Baym theory, and the next level of approximation assigned by $i+1$ is constructed from the i th approximation. Our algorithm of generating a series of approximations is almost the same as the one proposed by Takada [41]. Our scheme differs from Takada's one on three points; (1) we start with the Hartree approximation as an initial approximation, (2) we use the standard diagrammatic analysis for $\tilde{\Sigma}_\sigma(k)$ with respect to the *bare* or mean-field Green's function $G_\sigma^{(0)}(k)$ instead of the skeleton-expansion diagrammatic analysis with respect to the *dressed* Green's function $G_\sigma^{(i)}(k)$, and (3) we simplify iterative procedure by avoiding the Bethe-Salpeter equations. Our scheme is suitable to study the leading contribution of the vertex corrections.

(A) *The single-particle Green's function*: Suppose the excess self-energy $\tilde{\Sigma}_\sigma^{(i)}(k)$ is given as a functional of the mean-field Green's functions $G_\sigma^{(0)}$ ($\sigma =$

±), i.e.

$$\tilde{\Sigma}_{\sigma}^{(i)}(k) \equiv \tilde{\Sigma}_{\sigma}^{(i)}(k : [G_{\pm}^{(0)}]) \,. \tag{A.1}$$

We take the initial function as $\tilde{\Sigma}_{\sigma}^{(0)}(k) = 0$ (the Hartree approximation). Let the single-particle Green's function be

$$G_{\sigma}^{(i)}(k) = [G_{\sigma}^{(0)}(k)^{-1} - \tilde{\Sigma}_{\sigma}^{(i)}(k)]^{-1} \,, \tag{A.2}$$

where the corresponding diagram is shown in Fig. A.1 (a). $G_{\sigma}^{(i)}(k)$ is a function of $\tilde{\mu}_{\sigma}^{(i)}$; the particle number and chemical potential are calculated as

$$n_{\sigma}^{(i)} = \int_{k} \mathrm{e}^{\mathrm{i}\epsilon\eta} G_{\sigma}^{(i)}(k) \,, \tag{A.3}$$

$$\mu_{\sigma}^{(i)} = \tilde{\mu}_{\sigma}^{(i)} + \sum_{\sigma'} v_{\sigma\sigma'}(\mathbf{0}) n_{\sigma'}^{(i)} \,. \tag{A.4}$$

In this paper, we fix $\tilde{\mu}_{\sigma}^{(i)} \equiv \tilde{\mu}_{\sigma}$ during the calculation, and determine $\tilde{\mu}_{\sigma}$ by $n_{\sigma}^{(i)} = 3/4$ from a $\tilde{\mu}_{\sigma}$-n curve.

(B) *The vertex function*: Following the Kadanoff-Baym scheme, the vertex function $\Lambda_{\sigma\sigma'}^{(i)}(k;q) \equiv \Lambda_{\sigma\sigma'}^{(i)}(k;q : [G_{\pm}^{(0)}])$ is given as the sum of $\delta_{\sigma\sigma'}$ and all the possible diagrams obtained by inserting the external vertex carrying a momentum q into an arbitrary $G^{(0)}$-line with a spin σ' in each diagram for $\tilde{\Sigma}_{\sigma}^{(i)}(k : [G_{\pm}^{(0)}])$. This procedure is schematically shown by the Feynman diagrams in Fig. A.1 (b). Note that the wave numbers and the Matsubara frequencies at all the internal and external vertexes are conserved. The vertex function thus obtained satisfies various types of the Ward identity, one of which is given by

$$\Lambda_{\sigma\sigma'}^{(i)}(k;0) = \delta_{\sigma\sigma'} - \frac{\partial \tilde{\Sigma}_{\sigma}^{(i)}(k)}{\partial \tilde{\mu}_{\sigma'}} \,. \tag{A.5}$$

This identity is proved by the same way as in § 3.2.3 as follows. Since $\tilde{\Sigma}_{\sigma}^{(i)}(k)$ depends on $\tilde{\mu}_{\pm}$ only through $G_{\pm}^{(0)}$, the differential operation on $\tilde{\Sigma}_{\sigma}^{(i)}(k)$ with respect to $\tilde{\mu}_{\sigma}$ corresponds to an operation to pick up one internal $G_{\sigma'}^{(0)}(p)$ line in $\tilde{\Sigma}_{\sigma}^{(i)}(k)$ in all the possible ways, and to replaces it with $G_{\sigma'}^{(0)}(p)^2$. This differential operation is nothing but the vertex insertion for $q = 0$ as seen

in Fig. A.1 (b). (C) *The response functions*: The response function $\chi^{(i)}_{\sigma\sigma'}(q)$ is written in terms of the one-interaction irreducible part $\tilde{\chi}^{(i)}_{\sigma\sigma'}(q)$ at the i th level of approximation as

$$\chi^{(i)}_{\sigma\sigma'}(q) = \tilde{\chi}^{(i)}_{\sigma\sigma'}(q) - \sum_{\sigma_1,\sigma_2} \tilde{\chi}^{(i)}_{\sigma\sigma_1}(q) v_{\sigma_1\sigma_2}(\boldsymbol{q}) \chi^{(i)}_{\sigma_2\sigma'}(q)\,, \tag{A.6a}$$

$$\tilde{\chi}^{(i)}_{\sigma\sigma'}(q) = -\int_k G^{(i)}_{\sigma}(k+q) G^{(i)}_{\sigma}(k) \Lambda^{(i)}_{\sigma\sigma'}(k;q)\,. \tag{A.6b}$$

Then, the charge and spin response functions $\chi^{(i)}_{NN}(q)$ and $\chi^{(i)}_{S_zS_z}(q)$ are calculated as

$$\chi^{(i)}_{NN}(q) = \frac{1}{2}\sum_{\sigma,\sigma'} \chi^{(i)}_{\sigma\sigma'}(q), \tag{A.7a}$$

$$\chi^{(i)}_{S_zS_z}(q) = \frac{1}{2}\sum_{\sigma,\sigma'} \sigma\sigma' \chi^{(i)}_{\sigma\sigma'}(q). \tag{A.7b}$$

As proved in § 3.2.3, the Ward identity (A.5) leads the following identity between the isothermal susceptibilities and the q-limit of the response functions at the i th level of approximation:

$$\chi^{(i)}_c \equiv \frac{1}{2}\frac{\partial n^{(i)}}{\partial \mu} = \chi^{(i)}_{NN}(0), \tag{A.8a}$$

$$\chi^{(i)}_s \equiv \frac{1}{2}\frac{\partial m^{(i)}}{\partial h} = \chi^{(i)}_{S_zS_z}(0). \tag{A.8b}$$

(D) *The self-energy in the next level of approximation*: For a systematic improvement in the approximation, we require that the vertex functions should be taken account in a manner consistent with the single-particle Green's function. This requirement makes us to select the self-energy in the next level of approximation as

$$\tilde{\Sigma}^{(i+1)}_{\sigma}(k) = -\sum_{\sigma'}\int_q G^{(i)}_{\sigma}(k+q) V^{(i)}_{\sigma\sigma'}(q) \Lambda^{(i)}_{\sigma\sigma'}(k;q)\,, \tag{A.9a}$$

where the effective interaction $V^{(i)}_{\sigma\sigma'}(q)$ is given by

$$V^{(i)}_{\sigma\sigma'}(q) = v_{\sigma\sigma'}(\boldsymbol{q}) - \sum_{\sigma_1,\sigma_2} v_{\sigma\sigma_1}(\boldsymbol{q}) \tilde{\chi}^{(i)}_{\sigma_1\sigma_2}(q) V^{(i)}_{\sigma_2\sigma'}(\boldsymbol{q})\,. \tag{A.9b}$$

The diagrams of these equations are shown in Fig. A.1 (c) and (d). With this $\tilde{\Sigma}_\sigma^{(i+1)}(k) \equiv \tilde{\Sigma}_\sigma^{(i+1)}(k : [G_\pm^{(0)}])$, we can construct the approximation for $\chi_{NN}^{(i+1)}(q)$ and $\chi_{S_zS_z}^{(i+1)}(q)$ following the processes in (A), (B) and (C).

In the text, we have used two approximations, i.e., the RPA and the approximation with leading vertex corrections. In the iterative approximation described above, the former corresponds to $i = 0$, and the latter to $i = 1$. In principle, we can continue the iterative process as one hopes, although it is difficult to continue it for $i \geq 2$ practically. We note that response functions approaches the exact ones in the limit of $i \to \infty$ as [41]

$$\lim_{i\to\infty} \chi_{NN}^{(i)}(q) = \chi_{NN}(q)\,, \tag{A.10a}$$

$$\lim_{i\to\infty} \chi_{S_zS_z}^{(i)}(q) = \chi_{S_zS_z}(q)\,. \tag{A.10b}$$

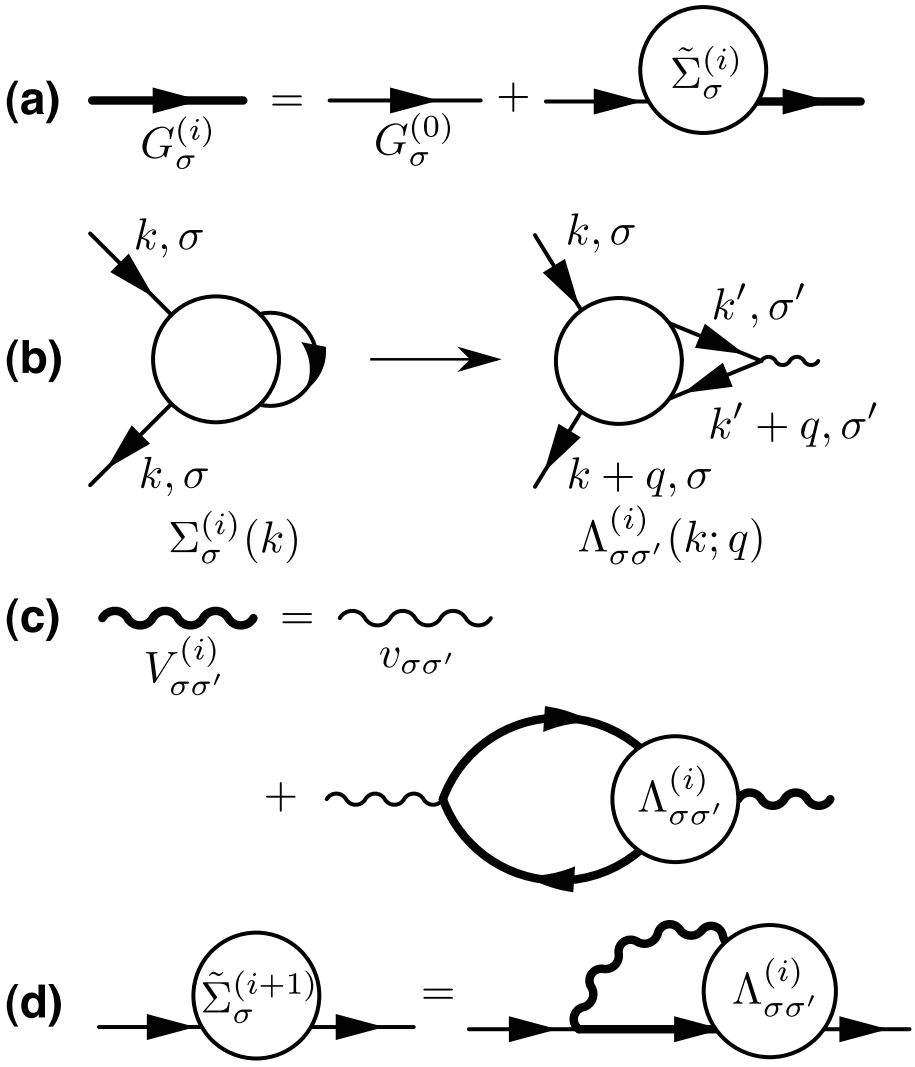

Figure A.1: The Feynman diagrams of the present iterative approximation: (a) the Dyson equation, (b) construction of the vertex function, (c) the effective interaction, and (d) the next definition of the self-energy.

Bibliography

[1] H. Seo, C. Hotta and H. Fukuyama: Chem. Rev. **104** (2004) 5005.

[2] K. Hiraki and K. Kanoda: Phys. Rev. Lett. **80** (1998) 4737.

[3] T. Takahashi, Y. Nogami and K. Yakushi: J. Phys. Soc. Jpn. **75** (2006) 051008.

[4] H. Mori, S. Tanaka and T. Mori: Phys. Rev. B **57** (1998) 12023.

[5] M. Watanabe, Y. Noda, Y. Nogami and H. Mori: J. Phys. Soc. Jpn. **73** (2004) 116.

[6] M. Watanabe, Y. Noda, Y. Nogami and H. Mori: J. Phys. Soc. Jpn. **74** (2005) 2011.

[7] K. Miyagawa, A. Kawamoto and K. Kanoda: Phys. Rev. B **62** (2000) R7679.

[8] R. Chiba, K. Hiraki, T. Takahashi, H. M. Yamamoto and T. Nakamura: Phys. Rev. Lett **93** (2004) 216405.

[9] K. Yamamoto, K. Yakushi, K. Miyagawa, K. Kanoda and A. Kawamoto: Phys. Rev. B **65** (2002) 085110.

[10] K. Inagaki, I. Terasaki and H. Mori: Physica B **329** (2003) 1162.

[11] T. Mori: J. Phys. Soc. Jpn. **72** (2003) 1469.

[12] M. Kaneko and M. Ogata: J. Phys. Soc. Jpn. **75** (2006) 014710.

[13] S. Nishimoto, M. Shingai, and Y. Ohta: Phys. Rev. B **78** (2008) 035113.

[14] H. Watanabe and M. Ogata: J. Phys. Soc. Jpn. **75** (2006) 063702.

[15] C. Hotta: J. Phys. Soc. Jpn. **72** (2003) 840.

[16] R. Chiba, H. M. Yamamoto, K. Hiraki, T. Nakamura and T. Takahashi: Synth. Met. **120** (2001) 919.

[17] H. Kobayashi, R. Kato, A. Kobayashi, Y. Nishio, K. Kajita and W. Sasaki: Chem. Lett. (1986) 833.

[18] S. Kimura, H. Suzuki, T. Maejima, H. Mori, J. Yamaura, T. Kakiuchi, H. Sawa and H. Moriyama: J. Am. Chem. Soc. **128** (2006) 1456.

[19] S. Kimura, T. Maejima, H. Suzuki, R. Chiba, H. Mori, T. Kawamoto, T. Mori, H. Moriyama, Y. Nishio and K. Kajita: Chem. Commun. (2004) 2454.

[20] H. Mori: J. Phys. Soc. Jpn. **75** (2006) 051003.

[21] H. Mori: private communication.

[22] S. Niizeki, F. Yoshikane, K. Kohno, K. Takahashi, H. Mori, Y. Bando, T. Kawamoto and T. Mori: J. Phys. Soc. Jpn. **77** (2008) 024714.

[23] H. Seo, J. Merino, H. Yoshioka and M. Ogata: J. Phys. Soc. Jpn. **75** (2006) 051009.

[24] Y. Ohta, K. Tsusui, W. Koshibae and S. Maekawa: Phys. Rev. B **50** (1994) 13594.

[25] M. Calandra, J. Merino and R. H. McKenzie: Phys. Rev. B **66** (2002) 195102.

[26] R. Pieteg, R. Bulla and S. Blawid: Phys. Rev. Lett. **82** (1999) 4046.

[27] K. Hanasaki and M. Imada: J. Phys. Soc. Jpn. **74** (2005) 2769.

[28] H. Seo: J. Phys. Soc. Jpn. **69** (2000) 805.

[29] A. Kobayashi, Y. Tanaka, M. Ogata and Y. Suzumura: J. Phys. Soc. Jpn. **73** (2004) 1115.

[30] Y. Tanaka, Y. Yanase and M. Ogata: J. Phys. Soc. Jpn. **73** (2004) 2053.

[31] K. Kuroki: J. Phys. Soc. Jpn. **75** (2006) 114716.

[32] S. Onari, R. Arita, K. Kuroki and H. Aoki: Phys. Rev. B **73** (2006) 014526.

[33] J. Merino, A. Greco, N. Drichko and M. Dressel: Phys. Rev. Lett. **96** (2006) 216402.

[34] Y. Tanaka: Ph.D thesis, The University of Tokyo.

[35] K. Miyake and O. Narikiyo: J. Phys. Soc. Jpn. **63** (1994) 2042.

[36] K. Morita, H. Maebashi and K. Miyake: J. Phys. Soc. Jpn. **72** (2003) 3164.

[37] Y. Fuseya, H. Maebashi, S. Yotsuhashi and K. Miyake: J. Phys. Soc. Jpn. **69** (2000) 2158.

[38] G. Baym and L. P. Kadanoff: Phys. Rev. **124** (1961) 287.

[39] G. Baym: Phys. Rev. **127** (1962) 1391.

[40] L. Hedin: Phys. Rev. **139** (1965) A796.

[41] Y. Takada: Phys. Rev. B **52** (1995) 12708.

[42] K. Yoshimi, H. Maebashi, and T. Kato: in preparation.

[43] A. A. Abrikosov, L. P. Gorkov and I. E. Dzyaloshinski, *Methods of Quantum Field Theory in Statistical Physics* (New York, Dover, 1975).

[44] W. Metzner, C. Castellani and C. D. Castro: Adv. Phys. **47** (1998) 317.

[45] To obtain the exact relations, inclusion and exactness properties are required[41]. In our formalism, it is easily seen that inclusion property is satisfied for each iterations. While, the exactness property is satisfied under the condition $\lim_{i\to\infty} G^{(i)} = G$. In this limit, we can obtain the exact response functions.

[46] In RPA, another reentrant transition (metal $\rightarrow$ CO with further decreasing temperatures) occurs as shown by a small return of the transition line at lowest temperatures in Fig. 3.3. This reentrant transition seems to be suppressed in the 1NSCA, although one needs to calculate low-temperature regions more to clarify it.

[47] V. J. Emery and S. A. Kivelson: Physica C 209 (1993) 597.

[48] K. Penc and F. Mila: Phys. Rev. B **49** (1994) 9670.